1-1-2007

An investigation of the use of transmission ultrasound to guide minimally invasive thermal therapy

Elham Soleimankhani
Ryerson University

AN INVESTIGATION OF THE USE OF TRANSMISSION ULTRASOUND TO GUIDE MINIMALLY INVASIVE THERMAL THERAPY

by
Elham Soleimankhani
B.Sc., Azad University, Iran, 2001

A thesis
presented to Ryerson University
in partial fulfillment of the
requirement for the degree of
Master of Applied Science
in the Program of
Electrical and Computer Engineering.

Toronto, Ontario, Canada, 2007

Author's Declaration

I hereby declare that I am the sole author of this thesis.
I authorize Ryerson University to lend this thesis to other institutions or individuals for the purpose of scholarly research.

Elham Soleimankhani

I further authorize Ryerson University to reproduce this thesis by photocopying or by other means, in total or in part, at the request of other institutions or individuals for the purpose of scholarly research.

Elham Soleimankhani

Instructions on Borrowers

Ryerson University requires the signatures of all persons using or photocopying this thesis. Please sign below, and give address and date.

Abstract

AN INVESTIGATION OF THE USE OF TRANSMISSION ULTRASOUND TO GUIDE MINIMALLY INVASIVE THERMAL THERAPY

Elham Soleimankhani (B.Sc.)

M.A.Sc., Electrical and Computer Engineering Department,
Ryerson University, Toronto, 2007

Minimally Invasive Thermal Therapy (MITT) is an effective way for the treatment of localized cancer and could replace surgery, chemotherapy or radiation. During MITT, high temperatures in the range of 55-95 °C are produced locally in the target tissue or tumour, resulting in localized protein coagulation. A real-time imaging method is required to guide the procedure of thermal therapy. Ideally, this imaging modality should be noninvasive, inexpensive and easily used and interpreted. It is known that acoustic attenuation is sensitive to both the tissue temperature and the structural changes due to protein coagulation (the endpoint of any thermal therapy treatment) during thermal therapy. Transmission ultrasound imaging is a real-time imaging modality which measures the attenuation property of ultrasound. The goal of this work is to demonstrate the potential of ultrasound attenuation imaging during MITT to quantitatively monitor lesion formation dynamics. An important finding of the present study is that the temporal changes in acoustic attenuation during MITT follow a reproducible pattern in albumen phantoms and bovine liver tissue within the range of thermal therapy temperatures. After heating, the measured attenuation remains higher than the initial amount, suggesting that this irreversible increase is a result of the structural change due to protein coagulation.

Acknowledgments

I would like to express my thanks and appreciation to my supervisor Dr. Michael Kolios for the encouragement and skillful guidance he provided throughout this thesis and for helping me to pursue a higher education. I would also like to thank my committee members Dr. Carl Kumaradas whose comments were particularly helpful and Dr. Kristiina McConville for all of her time and advice.

Further, I would like to acknowledge the financial support of CFI (Canadian Foundation for Innovation) and NSERC (Natural Sciences and Engineering Research Council). I am also grateful to the Department of Electrical and Computer Engineering and Department of Physics at Ryerson University for providing an excellent environment for my research.

I must thank Mr. Arthur Worthington for his technical support and suggestions during this work, Mr. John kula from Imperium Inc. for his assistance in solving the problems with the AcoustoCam, Dr. Behrouz Soroushian for exchanging ideas on AcoustoCam's operation and Shawn Mondoux for his help with the Hydrophone and LabVIEW software. A big thank goes out to the rest of the Biomedical Physics Group at Ryerson University for all the help and support.

I would like to also thank my fellow graduate students and friends at the Department of Electrical and Computer Engineering and Physics. In particular, thanks are given to Farhad for being very supportive during my difficult times, Talieh for being a wonderful study partner and friend and Madhu for all her support and friendship. I also thank Ahmed, Mehrnaz, Nazanin, Omar, Robin, Sally and Sara who were great labmates and friends.

Finally, I would like to especially thank my sisters, my parents and my grandparents for their constant understanding, love and support.

I have been so lucky to have a lot of nice people around me. My time at Ryerson University has definitely been a wonderful experience for life.

Contents

List of Figures

List of Tables

Chapter 1

Introduction

1.1 Minimally Invasive Thermal Therapy

Minimally Invasive Thermal Therapy (MITT) is an effective way to destroy localized diseased tissue and could be used as a replacement to conventional surgery, systematic chemotherapy, or radiation. Comparing to other cancer treatment methods, MITT is less risky and less invasive as it causes minimal damage to the overlying or surrounding tissue. It also requires shorter recovery times and results in a decrease in treatment costs due to its decreased complexity and short treatment duration (Goldberg et al 2000). During MITT, high temperatures in the range of 55 °C to 95 °C are produced locally in the target tissue or tumour, resulting in irreversible protein coagulation in a target volume of tissue. Thermal ablation procedures use energy sources that destroy a tumour by using thermal energy. The volume of damaged tissue is conventionally called a "lesion" (Thomson et al 1989). Several thermal ablation techniques to destroy cancerous tissue have been investigated some of which will be presented in the next section.

1.1.1 Thermal Ablation Techniques

The most commonly used ablative techniques today include high intensity focused ultrasound, radio frequency ablation, laser ablation and microwave ablation. All of these methods produce tissue coagulation as a result of elevating the temperature within biological tissue and have received much recent attention as minimally invasive strategies for the treatment

of diseased tissue.

High Intensity Focused Ultrasound (HIFU)

When a high-power ultrasound beam is focused onto a small focal region within the body, it produces an intense temperature elevation in the target tissue, resulting in tissue ablation. Ultrasound causes tissue damage through two predominant mechanisms. The first is by the conversion of mechanical energy into heat, the second is through cavitation due to bubble formation within the tissue. Due to the low intensity of the ultrasound beam in the intervening body tissue, the region within the focal zone can be targeted, preventing the nearby normal tissue from getting damaged (Yang et al 1993). In HIFU, the energy source is located outside the body and, consequently, no surgical incision is required (Figure 1.1). HIFU has been

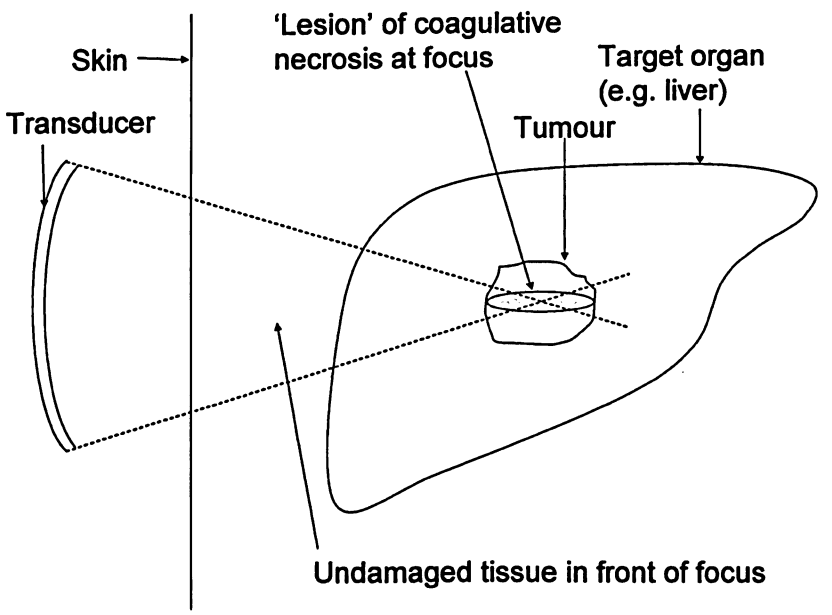

Figure 1.1: A schematic representation of high intensity focused ultrasound lesion production (Kennedy et al 2003).

investigated since the early 1950s as an effective approach to heat and destroy diseased tissue at depths up to 10 cm and at exposure times on the order of seconds (Fry et al 1950, 1954,

Lele 1967). Several investigations have been done to study high intensity focused ultrasound to produce focal lesions (ter Haar 1995, Wu et al 2003, Kennedy et al 2003, Murat et al 2006).

Radio Frequency Ablation (RFA)

Radiofrequency for electrocautery devices have been used for more than 70 years to achieve hemostasis during surgical procedures. Radio frequency Ablation is a thermal therapy treatment in which an alternating electrical current with frequencies in the range of 375 kHz to 500 kHz is applied to the tumour mass . This range of frequency is preferred to avoid depolarizing muscles and nerves during the heating. As high frequency alternating current flows to the surrounding tissue, the tumour mass gets heated due to the friction as ions in close proximity begin to oscillate at the applied frequency. This leads to irreversible coagulation of tissue. Advances in this technology have led to the development of instruments that may ablate larger volumes of tissue by thermal injury (Dickson and Calderwood 1983, Goldberg et al 2001, Dupuy and Goldberg 2001).

Laser Ablation

Laser ablation is a non-invasive treatment modality that uses thin, flexible fiber(s) inserted into the tumour mass to deliver optical energy to the diseased tissue. The laser light power is absorbed by the tissue and converted into heat. Temperatures above 55 °C are produced in the target volume (i.e. the tissue surrounding the laser fiber(s)). This temperature elevation leads to an irreversible coagulative cell death in the tumour mass (Figure 1.2).

Laser ablation was first introduced by Bown (1983) and has been investigated as a treatment modality for tumours (Roux et al 1992, Amin et al 1993, Beerlage et al 2000). Also, treatment planning models have been developed to gain an understanding of the optical and thermal propagation during interstitial laser photocoagulation and resultant tissue damage (Iizuka et al 2000, Jain 2006).

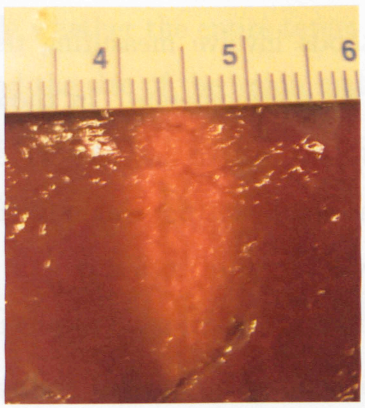

Figure 1.2: A laser-induced lesion in a piece of bovine liver tissue. The region of thermal coagulation can be seen as white in colour.

Interstitial Microwave Ablation

Microwave ablation devices consist of an applicator in the form of an antenna that emits microwaves with a typical frequency from 30 MHz to 30 GHz into the tissue to induce tumour destruction. Electromagnetic microwaves agitate water molecules in the surrounding tissue, producing friction and heat, thus inducing cellular death via coagulation necrosis. Microwave ablation devices could reach higher temperatures in shorter application times than RF ablation techniques since they are not limited by vapour formation (Goldberg et al 2005). Several groups have successfully applied microwave ablation in the treatment of cancerous tissue (Seki et al 2000, Lu et al 2001, Shock et al 2004).

1.2 Thermal Therapy Guidance

Limitations to current ablation techniques include the limited size of tissue coagulation zone and reduced performance next to large blood vessels. Therefore, a thermal therapy procedure should be guided through its stages by a point-based or image-based method or a combination of the two.

1.2.1 Point-based methods

Traditionally, point-based methods involve measuring temperature using thermocouples, thermistors, fluoroptic sensors or thermometers. In these methods the temperature sensors are invasively inserted into the tissue to measure the temporal changes in temperature. Increased accuracy could be achieved by introducing more measurement devices to the tissue which however increases the invasiveness of such methods. These methods are inexpensive. However, they are invasive and have a limited ability to be used in deep seated tissue regions.

1.2.2 Image-based methods

Image-based methods usually include visualizing the change in size and shape of the treated tissue throughout the procedure or monitoring a temperature-sensitive property of the imaging modality to indirectly estimate temperature variations. Clinical thermal therapy follows four distinct stages (Jolesz and Silverman 1995):

Planning refers to the procedure performed before thermal therapy treatment which helps to determine whether patient is suited for the therapy.

Targeting is the procedure of inserting the thermal therapy treatment applicator such as the laser fiber into the diseased tissue under imaging guidance e.g. ultrasound.

Monitoring includes observing the thermal therapy effects during the treatment delivery. A real-time monitoring method could prevent the nearby healthy tissue from getting damaged while treating the cancerous tissue by adjusting heating applicator location and power.

Controlling refers to the tools and techniques that are used to control the treatment based on the feedback of the monitoring devices.

Assessing the treatment response is the follow-up imaging performed after the thermal therapy procedure.

The above-mentioned terms could be classified as pre-interventional (planning), peri-interventional (targeting, monitoring, and controlling), and post-interventional (assessment of treatment response) (Clasen et al 2006).

Imaging thermal therapy effects in real-time to detect variations in size and shape of the lesion is very important to decide whether the entire target volume has been treated, i.e. to make sure whether the shape and the size of the lesion match those of the tumour.

The following section describes some of the imaging modalities which could be used to guide a thermal therapy treatment.

1.3 Image-Guided Thermal Therapy

In MITT a real-time imaging method is required to prevent the nearby normal tissue from damage during heating and to visualize the changes in size and shape of the diseased tissue throughout the treatment. Several imaging modalities have been investigated in the context of image-guided thermal therapy. These could be non-ionizing such as US or MRI, as they do not use ionizing radiation, or ionizing such as x-ray imaging and CT. An image-guided thermal therapy is preferable to point-based measurements (e.g. using thermocouples), since point-based methods are invasive. Point-based guidance methods can only be used in monitoring and controlling stages of a thermal therapy treatment and therefore they should be used along with an imaging modality for a successful thermal therapy treatment. Some of the common imaging modalities and how they could detect temperature and tissue structure variations during thermal therapy are as follows:

Computer tomography (CT) Computer tomography produces three-dimensional medical images from within the body using a series of two-dimensional X-ray images taken around a single axis of rotation. The CT scan may be done using "contrast agents", a substance taken by mouth or injected into an intravenous (IV) line that causes the particular organ or tissue under study to be seen more clearly by increasing the x-ray absorption. The CT scan could trace the blood flow changes as an indicator of thermal therapy progress as blood flow stops on the coagulated tissue. Computerized tomography has been investigated in thermal therapy guidance (Fallone et al 1982, Jenne et al 1997). The drawbacks to this imaging modality are that both patient and physician are exposed to ionizing radiation particularly

when multiple probe repositioning and ablations are anticipated. There is limited soft-tissue contrast. Also, most CT scanners do not have real-time capability and a specialized environment, usually in a hospital, is required (Cha et al 2000).

Magnetic Resonance Imaging (MRI) Magnetic Resonance Imaging is a medical imaging modality with exceptional soft-tissue contrast. MRI which was invented in the early 1970's uses radiofrequency waves and a strong magnetic field to provide detailed images of internal organs and tissues. MR imaging is sensitive to changes in both temperature and tissue microstructure that occur with thermal coagulation from heating.

The most common MRI methods for temperature measurement are based on temperature dependency of T1 (Parker et al 1983), T2 (Daniel et al 1999), and the Proton Resonance Frequency (PRF) (Ishihara et al 1992). PRF has seen more development as a thermometric method since it shows more linearity with temperature and it is not tissue dependent (Peters et al 1998). However, MRI is an expensive imaging modality, is not portable and may not be suitable for some patient populations, such as pregnant women, very large patients and also patients with pacemakers. Standard medical-grade stainless steel instruments cannot be used in MRI systems due to the relatively high magnetic field which is used in magnetic resonance scanners. Such instruments cause image artifact and are subject to torque and displacement in the magnetic field. Another drawback to typical MR imaging studies could be the fact that they can be time consuming.

Elastography Elastography, first introduced by Ophir (1991), is a non-invasive technique which maps information related to the elastic properties of the soft tissue. The resulting local changes in axial tissue strains due to heating are displayed as an image termed an elastogram. Soft tissues, generally, undergo more strain than harder tissues. The measured strain is related to the tissue shear modulus that is dependent on the tissue organization. Protein denaturation which is caused by the temperature elevation in thermal therapy changes the elastic modulus of the tissue. Qualitative results have been published on using elastography to investigate the effects of thermal therapy and depict the size and position of HIFU-induced lesions (Righetti et al 1999, Siebers et al 2003). Also, an investigation involving real-time

elastography detected a gradual increase in tissue stiffness following thermal damage in hyperthermia (Chen and Humphrey 1998).

Ultrasound (US) Ultrasound imaging is a real-time, non-invasive imaging modality with several temperature-sensitive properties. It is also portable and can easily be transferred from on location to the other to be shared among several examination rooms or taken to the patients' room when needed. Cost-effectiveness is another important advantage of ultrasound imaging systems, as these systems do not require special preparations such as shielding for x-ray imaging and a uniform magnetic field for MRI scanning. Also, an ultrasound imaging system can be used over a long period of time. As a result, one in four imaging studies uses ultrasound. It could therefore be used as a suitable imaging modality in all the steps of an image-guide minimally invasive thermal therapy as it has also shown to be temperature-sensitive (Mudry et al 2003).

The disadvantages of ultrasound imaging include:

1. The high reflection of the incident acoustic energy (upto 99.9 percent) at gas-soft tissue interfaces. As a result, images of tissues at the far side of the lungs are not possible to get.
2. There is poor soft tissue contrast compared to other imaging modalities.
3. It is operator dependent.
4. It is usually difficult to interpret and compare results from machine to machine.

1.4 Ultrasound

Ultrasound is any sound wave whose frequency is above the limit of human hearing, which is usually taken to be 20 kHz. It is conventionally produced when an electric field is applied across a piezoelectric crystal to induce a mechanical deformation. In this manner, the piezoelectric transducer converts an oscillating electric signal into an acoustic wave (a pressure wave). This phenomenon is called the inverse piezoelectric effect and was first demonstrated by Jacques and Pierre Currie in 1880. Some 35 years after piezoelectricity was discovered, ultrasonic imaging was developed by Paul Langevin and in the late 1940s, human body was

being imaged by ultrasonic techniques. The typical ultrasonic systems capture and display the echoes backscattered by structures within the body. These echoes are used to form images.

1.4.1 Ultrasound Properties in Interaction with Biological Tissue

Some of ultrasound properties in interaction with biological tissue are explained below:

Propagation Speed The speed of sound in tissue depends on the tissue compressibility and density and is usually measured in meters per second. The speed of ultrasound is given by:

$$c = \frac{1}{\sqrt{\rho\beta}} \tag{1.1}$$

where ρ is the density of the tissue in kg/m^3 and β is the compressibility of the tissue in Pa^{-1}.

Impedance The fraction of an incident sound wave on a boundary between two media that is reflected or transmitted depends on the relative impedances of the two materials (in a way similar to Snell's law in optics). Acoustic impedance is the product of acoustic density and acoustic propagation speed and is expressed in $kg/m^2.s$:

$$Z = \rho c = \sqrt{\rho/\beta} \tag{1.2}$$

Reflection Ultrasound reflection occurs at interfaces between large regions (much larger than a wavelength). The greater the difference between impedances of two materials, the more of the incident sound wave will get reflected. When ultrasound travels from one medium to the other and is perpendicular to the interface, the reflection coefficient at the boundary between the two media is given by:

$$R = \frac{Z_2 - Z_1}{Z_2 + Z_1} \tag{1.3}$$

In which Z_1 and Z_2 refer to acoustic impedances of the two media.

Table 1.1: Properties of certain soft human tissue at 37 °C (Duck et al 1998).

Tissue	Acoustic Impedance ($kg/m^2.s$)	Speed of Sound (m/s)	Attenuation Coefficient (dB/cm.MHz)
Air	$0.0004x10^6$	344	–
Lung	$0.018x10^6$	650	40
Fat	$1.34x10^6$	1460	0.61
Water	$1.48x10^6$	1480	0.0002
Kidney	$1.63x10^6$	1561	1.04
Blood	$1.65x10^6$	1570	0.18
Liver	$1.65x10^6$	1549	0.4-7.0
Muscle	$1.71x10^6$	1580	0.74
Bone	$7.8x10^6$	3500	14.0

Scattering Scattering of the ultrasound wave occurs when irregularities or inhomogeneities in the acoustic properties of a medium are comparable with or smaller than the wavelength of the sound. The part of the scattered pressure wave which gets reflected to the transmitter is termed backscatter.

Attenuation Ultrasound attenuation refers to the reduction in signal amplitude that occurs per unit distance traveled. Attenuation is the combined effect of scattering and absorption. The original ultrasound beam is constantly divided into partial waves at each inhomogeneity boundary within the tissue. These partial waves along their path are gradually converted into heat because of the pressure wave absorption. Absorption is the conversion of sound energy into heat. In a homogeneous medium the greater part of attenuation is the ultrasound absorption. The more inhomogeneous the medium, the more the scattering effect contributes to ultrasound attenuation.

1.5 Ultrasonic Attenuation Measurement

Ultrasound is attenuated exponentially as a function of distance or sample thickness as it travels through tissue:

$$I_2 = I_1 e^{-\alpha_{Np}\Delta x} \tag{1.4}$$

and therefore:

$$\alpha_{Np}\Delta x = \ln \frac{I_1}{I_2} \tag{1.5}$$

I_2 is the attenuated sound pressure wave intensity after it travels through a section of length Δx and I_1 is the sound pressure wave intensity before it gets attenuated. α_{Np} refers to the acoustic attenuation coefficient.

The decibel measure is obtained if the logarithm to the base 10 is used and multiplied by 20. The two forms of attenuation are related by:

$$\alpha_{dB}\Delta x = 20\log_{10} \frac{P_1}{P_2} \tag{1.6}$$

The following equation indicates how the two units for ultrasonic attenuation (i.e. dB and Np) could be converted from one to the other:

$$\alpha_{dB} = 8.686\alpha_{Np} \tag{1.7}$$

Higher frequencies are desirable to achieve better spatial resolution. However, the highest frequency which could be used for imaging is limited by the fact that acoustic attenuation increases with frequency and therefore a tradeoff must be made between the ultrasound frequency and the total resultant attenuation value for the tissue. The frequency-dependent attenuation obeys a power law:

$$\alpha = af^n \tag{1.8}$$

where α is the attenuation coefficient expressed in dB/cm, a and n are tissue-dependent constants and f refers to the frequency of the ultrasound in MHz. For tissues, n varies from 1 to 2.

Figure 1.3 shows the attenuation values for various biological tissues. Different biological tissues attenuate the ultrasound by different amounts. For instance, 2 cm of liver tissue will attenuate the sound wave by 4 dB at 5 MHz. Also, blood has the least and bone has the highest attenuation value amongst all tissues.

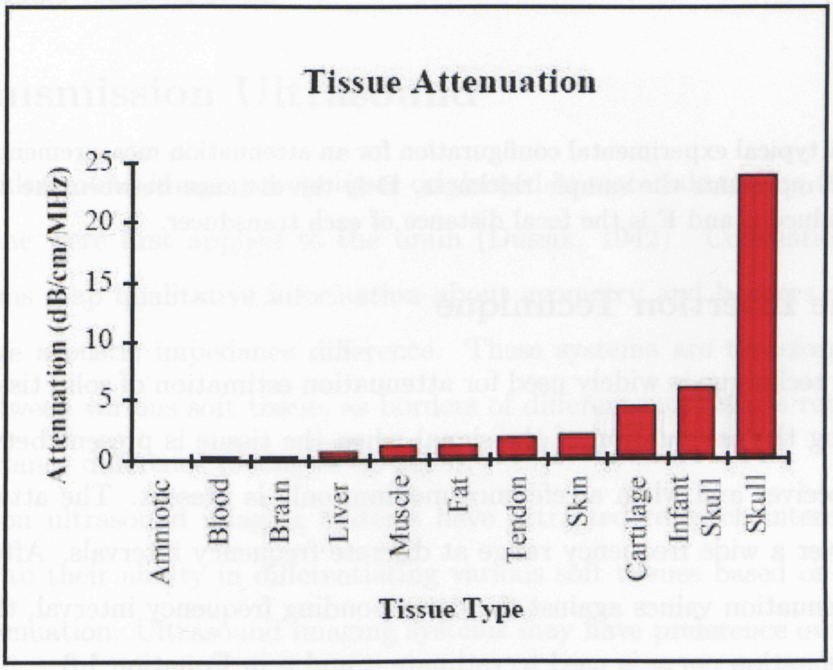

Figure 1.3: A summary of ultrasound attenuation for various biological tissues. (J. Brian Fowlkes, 1999)

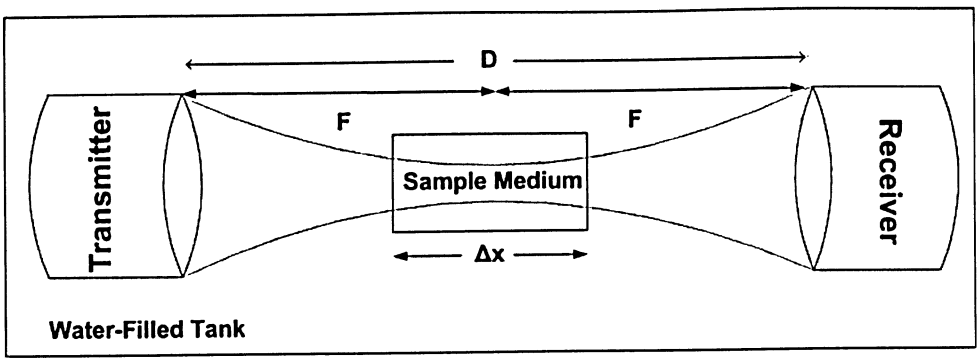

Figure 1.4: A typical experimental configuration for an attenuation measurement by the insertion technique. Δx represents the sample thickness, **D** is the distance between the transmitting and receiving transducers, and **F** is the focal distance of each transducer.

1.5.1 The Insertion Technique

The insertion technique is widely used for attenuation estimation of solid tissues. It is based on determining the attenuation of the signal when the tissue is present between the transmitter and receiver and when a reference medium only is present. The attenuation can be determined over a wide frequency range at discrete frequency intervals. After graphing the measured attenuation values against the corresponding frequency interval, the least squares fit to the attenuation curve is used to estimate a and n in Equation 1.8.

Figure 1.4 shows the setup used for attenuation measurement by the insertion technique. The setup consists of two transducers. One acts as a transmitting transducer and sends ultrasound pressure waves through the sample medium. The other one is a receiving transducer and receives the attenuated ultrasound pressure wave after it travels through the coupling medium and specimen which is located between the two transducers. Equation 1.6 is then used to calculate the attenuation value for the particular sample medium of thickness Δx.

Disadvantages of the insertion technique are that reflections at the specimen faces are included in the measured losses and it is difficult to accurately cut parallel sided tissue slabs. Using two samples of the same material but of varying thickness could eliminate the reflec-

tion losses. The attenuation coefficient could thus be calculated by the following equation:

$$\alpha_{dB} = \frac{-20}{\Delta x} \log_{10} \frac{P_2}{P_1} \tag{1.9}$$

where α is the attenuation coefficient in dB/cm, Δx is the thickness difference of the two samples in meters. P_2/P_1 is the ratio of attenuated pressure wave amplitude through the thicker and thinner tissue samples.

1.6 Transmission Ultrasound

Transmission ultrasound imaging techniques originated in materials testing (Sokolov, 1929), and in medicine were first applied to the brain (Dussik, 1942). Conventional pulse-echo imaging systems map qualitative information about geometry and borders of tissue where there is a large acoustic impedance difference. These systems are therefore less sensitive to changes between various soft tissue, as borders of different soft tissues represent a small acoustic impedance difference (Jeong et al, 2005).

Transmission ultrasound imaging systems have attracted research interest in the past few years due to their ability in differentiating various soft tissues based on their speed of sound and attenuation. Ultrasound imaging systems may have preference over conventional pulse-echo imaging techniques as they can provide more quantitative information about soft tissue within human body depending on the specific application.

Transmission ultrasound imaging could provide a linear projection of tissue attenuation property. Spatial mapping of attenuation is useful where a comparison of regions of normal and pathological tissue is required (Figure 1.5). Figure 1.6 shows how transmission ultrasound could be used to detect small vessels and fibrotic tissue of the finger.

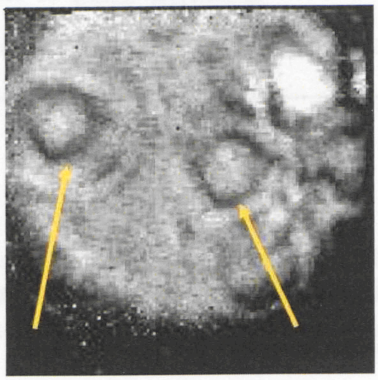

(a) Two cysts in a breast-mimicking phantom.

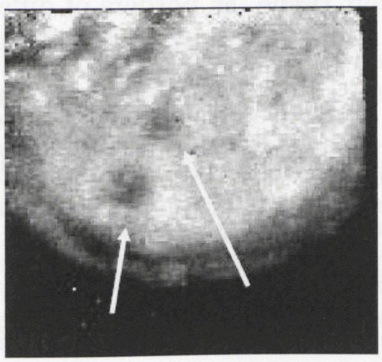

(b) Two masses in a breast-mimicking phantom.

Figure 1.5: Transmission ultrasound images of a breast-mimicking phantom containing cysts and masses (Lo et al 2005).

Figure 1.6: Attenuation image of a pointing finger tip taken with AcoustoCam at 7.5 MHz. Small vessels and fibrotic tissue could be seen on the image (Lo et al 2005).

1.7 Ultrasound imaging as a method to guide thermal therapy

Ultrasound has several temperature-sensitive properties that can be used for monitoring thermal therapy. Several of these properties will be examined in the next few paragraphs.

1.7.1 Temperature-sensitive properties of ultrasound

Ultrasound Backscatter

Changes in backscattered energy due to heating are dependent on the type of the inhomogeneity which causes the scattering (Straube et al 1994). Increased echogenicity of the soft tissue during thermal therapy is attributed to gas bubble formation due to vaporization and/or cavitation (Hynynen 1991, Gertner et al 1998). However, this increased echogenicity tends to decrease with time (Watkin et al 1995), presumably due to the resorption of the bubbles. The hyperechoic region, therefore, could be detected on conventional sonograms only in a few cases, and the results do not seem to be consistent. The sensitivity to noise has yet to be fully determined for change in backscattered energy calibration data as noise is inevitable in in-vivo experiments. This sensitivity will determine the temperature accuracy that is possible for a given spatial resolution. It has been demonstrated that ultrasound backscatter coefficient is the least useful acoustic parameter to visualize a heat-induced lesion (Bush et al 1993).

Ultrasonic propagation speed

The speed of sound through tissue is determined principally by tissue density and compressibility (ranging from 1460 m/s for fat to 3500 m/s for bone), and is the primary ultrasonic parameter which has been used in the early works on temperature measurement (Bowen et al. 1979, Rajagopalan 1979, Prakash 1980). Sound speed in fatty tissue generally decreases with temperature (Bamber and Hill 1979), while it increases in non-fatty tissue with temperature, peaks at 50-60 °C, and then decreases as temperature further increases (Figure 1.7). Methods based on speed of sound have not been implemented clinically yet. One reason is

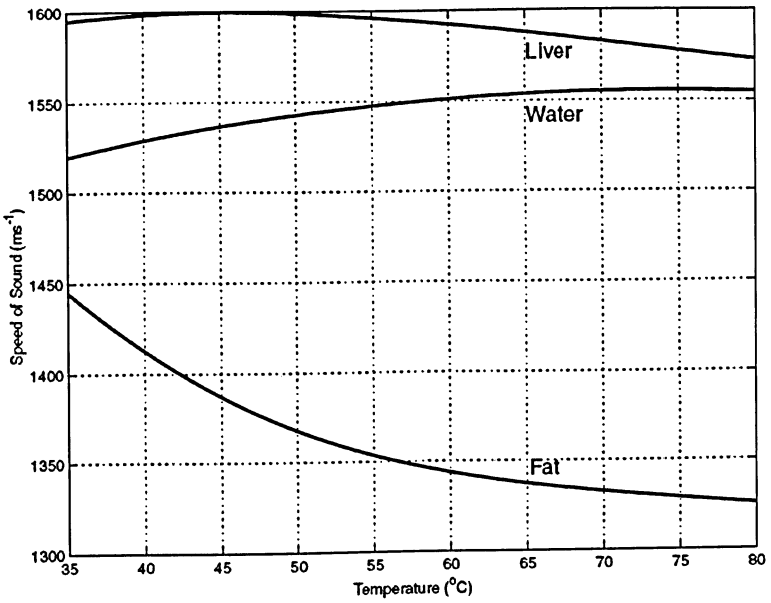

Figure 1.7: Temperature dependence of sound speed in soft tissue (adapted from Connor and Hynynen 2002)

the necessity of measuring both distance and time to image an identifiable target from two directions or to use a crossed-beam (multiple beams) method (Ophir 1986). These type of measurements are further complicated due to the fact that ultrasonic windows which are required to allow the insonification of a region of interest from two views do not always exist in vivo. Also, depending on the tissue type, e.g. the amount of water or fat content of the soft tissue, temperature dependence of the speed of sound (SOS) differs.

Ultrasonic Attenuation Coefficient (UAC)

The ultrasound attenuation coefficient strongly changes with temperature. The reversible attenuation changes are due to temperature dependence of water attenuation (Figure 1.8) and the irreversible changes are due to changes in tissue structure. The attenuation coefficient

change is more pronounced at temperatures over 50 °C where a coagulative tissue necrosis starts to occur. Recording the attenuation coefficient change could result in a higher signal to noise (S/N) ratio as compared to backscattered ultrasound (Bamber and Hill 1979). In a study of measuring the change in backscattered coefficient, speed of sound and attenuation coefficient with temperature rise in biological tissue, it was demonstrated that attenuation coefficient was the most useful acoustic parameter to visualize a heat-induced lesion (Bush et al 1993).

When soft tissues are heated beyond 40-50 °C, marked increases in the attenuation

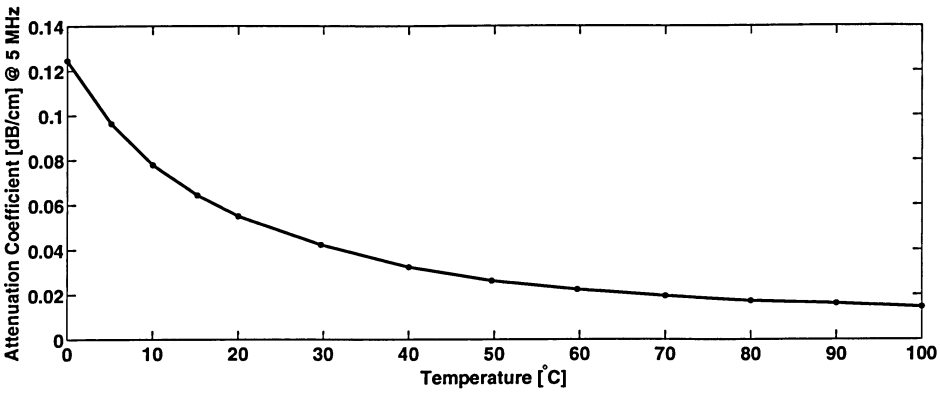

Figure 1.8: The attenuation variation versus temperature for water. (Attenuation values were recalculated from the original graph (Pinkerton 1949) to be presented in dB/cm units.)

coefficient are seen to occur as the temperature is further increased. For example, when heating from just above 50 °C to about 80 °C, the attenuation coefficient at 4.2 MHz in cat brain in vivo was observed by Robinson and Lele (1972) to increase about five-fold, compared with a decrease of just a few percent when the temperature was raised from 30 °C to 50 °C. Gertner et al (1997) found a US attenuation coefficient increase by 1.48 dB/cm in a bovine liver sample over a 30 minute period at 70 °C. The general attenuation increase is in agreement with the previous data obtained from canine (Damianou et al 1995) and bovine (Bamber et al 1977) tissue heating. In another study by Bamber and Hill (1979) it was found that the attenuation of excised liver tissue with temperature in the range of 5-55 °C decreased and then increased until it reached 65 °C and remained constant at 65 °C. In

a study of dog muscle, liver and kidney, Damianou et al (1997) could detect an attenuation coefficient increase of 0.36 dB/cm.MHz in a temperature range of 50 °C to 70 °C (Figure 1.9).

In another study the US attenuation coefficient change with heating in samples of hu-

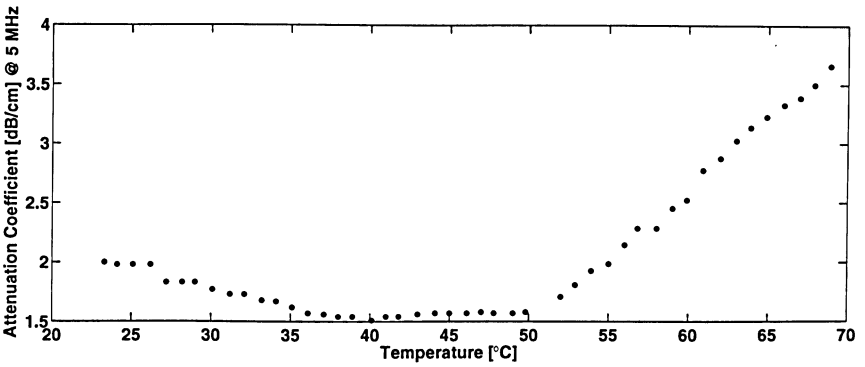

Figure 1.9: Attenuation coefficient versus temperature for liver in vitro. (adapted from Damianou et al 1997 and recalculated to be presented in dB/cm units)

man prostate was measured. No significant change was observed at temperatures below 55 °C. Worthington et al (2002) found an attenuation increase of 1.25 dB/cm and 2.7 dB/cm at a frequency of 5 MHz at heating temperatures of 60 °C and 65 °C, respectively. It can be concluded that heating different types of biological tissue to temperatures above 50 °C results in an overall increase in attenuation coefficient.

1.8 Spatial Mapping of Ultrasonic Attenuation

Several investigators have studied the use of transmission ultrasound to map acoustic attenuation for tissue imaging.

In a method introduced by Calderson et al. (1976) attenuation images of inserted samples were provided. In this method, a scanned-laser interferometer was used to measure the displacement amplitude of a fine membrane that had been excited to vibrate by a short transmitted acoustic pulse. Computerized reconstruction from one-dimensional ultrasonic projections could provide images of the attenuation coefficient. The presence of artefact due

to refraction and phase cancelation is a major drawback to this type of imaging (Carson et al. 1981, Greenleaf and Bahn 1981, Klepper and Brandenburger 1981).

A High-Resolution Ultrasonic Transmission Tomography (HUTT) system was invented for three dimensional interphantom/intraphantom tissue classification based on acoustic attenuation profile of biological tissue. The system could detect tiny structures inside a bovine kidney and sheep kidneys as well as chicken tissue, calyces and vessel-duct successfully. The tissue differentiation was performed using a set of CEM (Constrained Energy Minimization) filters (Jeong et al 2005). Five transmission ultrasound cameras which were used in tissue imaging are to be mentioned:

1. The first transmission ultrasound camera developed at the the Stanford Research Institute (Green et al. 1974) used a unique acoustic system consisting of an acoustic lens and a linear, one-dimensional array as the receiver in a fixed position. The scanning resolution in the second dimension was obtained by a complex system of rotating prisms. This system could provide real-time images of in-vivo and in-vitro soft tissue such as colon, kidney and liver. The obtained images needed further improvement to be used for clinical purposes because the frame rate was limited when imaging in real-time.

2. A transmission ultrasound camera based on the same concept as the camera developed at Stanford Research Institute was designed by Brettel et al (1981). The only difference was that the second dimension was achieved by mechanical movement of the receiving array instead of a system of rotating prisms. This camera could not provide real-time images due to the mechanical movements.

3. Siemens AG developed a transmission ultrasound camera which was used in several studies for real-time imaging. The setup was very similar to the one designed at the Stanford Research Institute camera. The receiving array was a two-dimensional PVDF array with 128 by 128 elements. The drawback of this imaging system was the high costs for the complicated receiving array with its 16384 transducers, preamplifiers and signal paths to the multiplexer (Granz 1982, Oppelt and Ermert 1984, Granz and Oppelt 1987).

4. Ermert et al (2000) and Keitmann et al (2002) studied an ultrasound transmission camera

which could provide real-time images of moving joints and tendons with an image quality similar to the one obtained with Siemens camera. This new camera used a number of 256 array elements which considerably reduced the costs for the production of this camera. A phased array on the transmitting side generated a vertical focal line which swept across the focal plane with a frequency of 25 Hz and a 128 element array with an acoustic lens was used on the receiving side. The only drawback was the lens artifact which affected the image quality.

5. AcoustoCam is a transmission ultrasound camera which was developed at Imperium Inc.. This innovation is a two dimensional imaging system that creates real-time, high-resolution images of subsurface structures (Lasser et al 1996, Lasser 1997). The transmitting transducer is an unfocused planar transducer which is responsive over a wide frequency range from 1 to 10 MHz. The receiving part consists of an array with $128 \times 128 = 16383$ pixel elements and a compound acoustic lens to focus the ultrasound pressure wave onto the array. The use of AcoustoCam for tissue imaging has been investigated in several studies, to examine its potential in medical imaging (Lo et al 2005) and to study the effects of temperature elevation on biological tissue (King et al 2003, Parmar and Kolios 2006).

1.8.1 Previous Work on Spatial Mapping of Attenuation to guide Thermal Therapy

Several studies have investigated the effect of temperature increase on images based on attenuation coefficients. In one study, lesions were generated by high intensity focused ultrasound in pig liver specimen and two dimensional images of the mean attenuation coefficient of the lesion as a function of frequency in the range of 3 to 8.5 MHz were created. These attenuation images were then compared to the photographic images of the lesion and showed to provide useful qualitative information. Quantitatively, a significant increase in attenuation coefficient of the lesion relative to normal tissue was detected (Bush et al. 1993). The transmission ultrasound camera (AcoustoCam) was used by King et al. (2003) to record acoustic images before, during and after tissue heating with high intensity focused ultrasound. It was

concluded that the camera was sensitive to acoustic attenuation changes during heating and could detect the effects of tissue coagulation. However, the attenuation values were estimated based on pixel intensity variation only and the camera was not calibrated in terms of attenuation. Parmar and Kolios (2006) used the same camera to investigate the effects of thermal therapy and could find a general increase in attenuation coefficient during heating. They found out it was difficult to localize the attenuation increase inside the tissue, but their work provided the first quantitative measurements using this technology. However, their work was limited by calibrations based on phantoms with assumed ultrasonic properties.

1.9 Summary

Real time image guidance for minimally invasive thermal therapy increases the treatment effectiveness in all of the MITT stages including: pre-interventional planning, peri-interventional targeting, monitoring, controlling and post-interventional assessment of the treatment response. Ultrasound imaging is an imaging modality with several properties sensitive to temperature elevations and bulk tissue changes. There are some characteristics of an ultrasound imaging system which make it advantageous over other imaging modalities to guide a thermal therapy treatment: it does not disturb the presence of the heating device, it is non-invasive, portable and cost-effective.

Several investigations of temperature sensitive properties of ultrasound in interaction with biological tissue indicate that attenuation is subject to significant change in temperatures in the range of 50 °C and 90 °C in which tissue coagulative necrosis occurs. During tissue heating, the increase in the temperature of the water content of biological tissue tends to decrease acoustic attenuation, especially up to 60 °C (Figure 1.8), while tissue coagulation which occurs in temperatures over 60 °C increases tissue acoustic attenuation.

Transmission ultrasound imaging is capable of detecting the combined effect of attenuation variations of tissue due to water heating and tissue coagulation. It measures the attenuated pressure wave after ultrasound propagates through the tissue and could give a good quantitative estimation of tissue properties. It is capable of distinguishing between

various soft tissues and has proved to be an effective way in tissue differentiation (Jeong et al., 2005).

This study involves the investigation of using a transmission ultrasound camera (AcoustoCam, Imperium Inc., Silver Spring, MD) to estimate the acoustic attenuation change during thermal therapy. This study is an improvement compared to other studies since:

a. The attenuation coefficients of the tissue-mimicking phantoms used to calibrate the AcoustoCam were measured by an independent method, instead of assuming values based on phantom composition.

b. Attenuation changes as a function of thermal dose were investigated.

c. The AcoustoCam array used in this study has better SNR compared to its predecessor.

It is known that acoustic attenuation is a temperature-sensitive property of ultrasound. This thesis investigates the use of AcoustoCam to detect the attenuation variations with temperature. The second chapter is an introduction to the AcoustoCam setup and its calibration procedure including tissue mimicking phantom construction and an insertion technique which independently measures the acoustic attenuation of the constructed phantoms. In the third chapter, the experimental results of extracting the image data for the set of PVCP tissue-mimicking phantoms are correlated to the acoustic attenuation for each phantom. The established relationship is used to assess the attenuation behaviour of albumen phantoms and bovine liver tissue within the typical thermal therapy temperature range. The last chapter includes the discussion and future work.

Chapter 2

Methods

2.1 AcoustoCam Ultrasonic Camera

The AcoustoCam ultrasonic camera is an attenuation-based ultrasound system which is developed by Imperium Inc. (Silver Spring, MD) and employs a patented technique that allows collection of wide area ultrasonic images of an object in a similar way that a digital camera captures light images. This transmission ultrasound camera as illustrated in Figure 2.1 consists of three major parts:

1. **The transmitting transducer** is a non-focused planar transducer (2.54 cm diameter) which is operated at 3.5 MHz - 7 MHz frequency and produces unfocused planar ultrasound waves that is attenuated by the sample medium.

2. **The acoustic compound lens** consists of two acoustic lenses. It is an inexpensive and simple alternative to focus the ultrasound beam onto a small region of the receiving array.

3. **The ultrasound sensing system (Receiving array)** consists of a silicon readout array and a PE-CMOS array which is responsive over a wide frequency range. The PE-CMOS array is a piezoelectric material deposited onto a CMOS array. It has 128 by 128 pixel elements and an active size of 1 cm^2. The whole setup as shown in Figure 2.1 should be placed in a glass tank filled with degassed water.

Figure 2.2 shows the schematic of the AcoustoCam. The front lens of the acoustic compound lens is in a fixed position, while the rear lens moves using a focusing knob on the side of the camera body to achieve a good focus. The array is located behind the rear lens and the

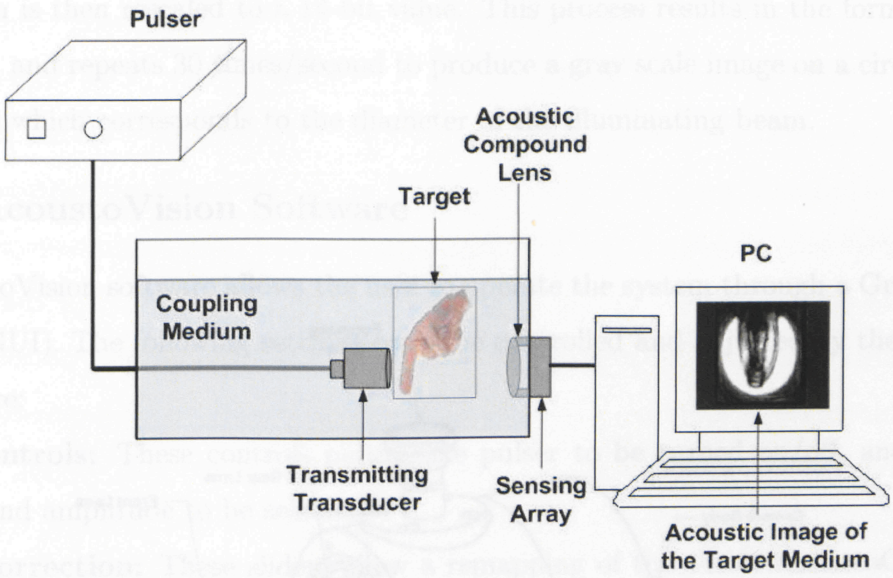

Figure 2.1: The AcoustoCam Setup consists of three parts: an unfocused transmitting transducer, a compound acoustic lens system and a receiving array.

chamber between them is open. The open chamber becomes flooded as the water tank gets filled.

2.1.1 Image Acquisition

The ultrasonic burst pulser sends pulses to the unfocused transmitting transducer to produce highly uniform plane ultrasound waves. The plane ultrasound wave travels through the target, gets attenuated and after striking the acoustic lens system is focused onto the sensor array. The focused ultrasound exerts a pressure upon the piezoelectric coating of the sensor array which will be converted to a time-varying signal. The ReadOut Integrated Circuit (ROIC) that is attached to the centre of the of the array is a patented, custom-designed circuit that contains 120×120 cells or pixels. Each pixel contains the necessary circuitry to

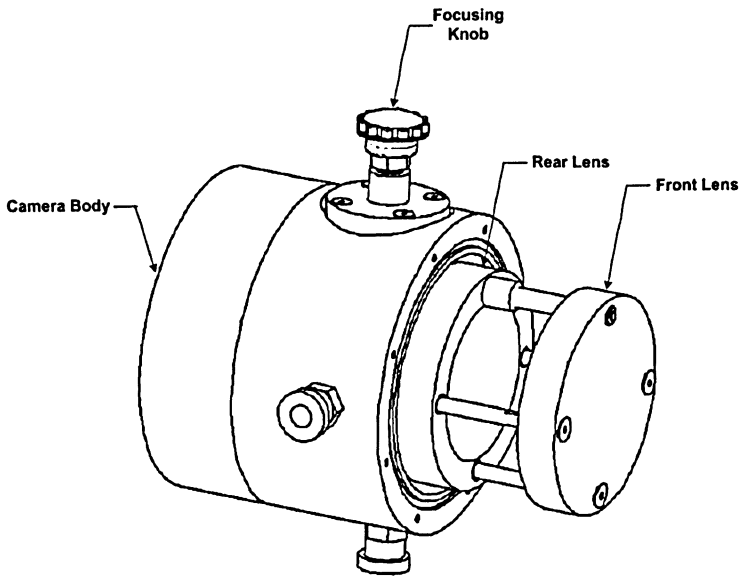

Figure 2.2: Schematic of AcoustoCam's head which incorporates two acoustic lenses. The front lens is in a fixed position. To focus at other distances, the rear element is moved with the sensor fixed in place. The fixed distance between the front flat lens surface and the sensor is 8.6 cm.

detect and capture the electrical signals that are generated by the piezoelectric elements. Each datum is then rescaled to a 14-bit value. This process results in the formation of the image data, and repeats 30 times/second to produce a gray scale image on a circular shaped background which corresponds to the diameter of the illuminating beam.

2.1.2 AcoustoVision Software

The AcoustoVision software allows the user to operate the system through a Graphical User Interface (GUI). The following settings could be controlled and adjusted by the AcoustoVision software:

Pulser Controls: These controls permit the pulser to be turned on/off, and the pulser frequency and amplitude to be selected.

Display Correction: These sliders allow a remapping of the 14-bit AcoustoCam sensor's output consisting of 16,384 levels for presentation within the 8-bit monitor display with 256 different gray levels.

Acoustic Path Distance: Using this slider, the distance from the transducer to the detector will be specified in order to establish the time period at which the detector is active.

Two types of data could be acquired from AcoustoCam:

1. 8-bit data which is the pixel intensity of the image displayed on the screen. The data ranges between 0 and 255, resulting in 256 gray levels.

2. 14-bit data which is the output of the AcoustoCam's sensor array, ranges between 0 and 16383, and could be acquired by the AcoustoVision software. The RS-232 serial link application window in the AcoustoVision allows the user to extract the 14-bit data from the AcoustoCam's sensor. However, the 14-bit data from each individual pixel cannot be extracted and the 14-bit data extracted is an average of the pixel intensities within the displayed region.

2.1.3 Tissue-Mimicking Phantom Construction with PVCP

To obtain quantitative data, the AcoustoCam must be first calibrated with samples of known attenuation called tissue-mimicking phantoms. A tissue-mimicking (TM) phantom refers to a sample medium which simulates the characteristics of the biological tissue. In the present study, these phantoms were required to simulate a range of acoustic attenuation. Constructing tissue-mimicking phantoms is of importance in AcoustoCam's calibration procedure and could help to determine how acoustic attenuation is related to the image data, i.e. mean pixel intensity. The ultrasonic attenuation values for the phantoms need to cover a range of acoustic attenuation as different biological tissues have different acoustic attenuation values.

PVCP (Polyvinyl Chloride Plastisol, MF Manufacturing Co., Fort Worth, Texas, USA) is a non-toxic white opaque plastic solution which was used for TM phantom construction in this study. It is insoluble in water, is homogeneous and could be kept and reused for a long period of time without any degradation in its properties. To make the TM phantoms, PVCP stock solution was heated to 200°C and was stirred continuously during the heating process in order to get a homogeneous heat distribution. The stirring process should be performed gently to prevent air bubble formation, as air bubbles strongly attenuate ultrasound and cause large inhomogeneities within the sample medium. The white plastic solution turns to a translucent yellowish colour liquid upon heating and is ready to be poured into the desired molds.

Based on previous studies using PVCP (Gloria Spirou 2005) and considering the linear relationship between total attenuation and the attenuation coefficient, it was calculated that phantom thicknesses as indicated in Table 2.1 should be used to produce ten tissue-equivalent phantoms with attenuation values in the range of 3 dB and 30 dB at 4.76 MHz. For this purpose, PVC piping was cut into the calculated lengths which were then used as molds. Each mold was clamped between two pieces of glass and the heated PVCP stock solution was poured into the mold through a hole which was drilled into the piping.

Upon cooling, PVCP solidifies and could be used in direct contact with water for attenuation

Table 2.1: PVCP Phantom Thickness Estimation

Phantom	Thickness (cm)
Phantom A	0.52±0.05
Phantom B	1.17±0.05
Phantom C	1.71±0.05
Phantom D	2.42±0.05
Phantom E	3.07±0.05
Phantom F	3.72±0.05
Phantom G	4.30±0.05
Phantom H	4.93±0.05
Phantom I	5.45±0.05
Phantom J	6.30±0.05

measurement and scanning purposes. Prolonged contact of PVCP with other plastics should however be avoided as PVCP reacts with and dissolves other plastic materials. Figure 2.3 shows a photograph of the constructed PVCP TM phantoms.

2.1.4 PVCP TM Phantom Attenuation Measurement

The insertion technique described in Section 1.5.1 was employed to independently measure the acoustic attenuation of the constructed TM phantoms.

An attenuation measurement setup as in Figure 2.4 was built using two 5-MHz focused transducers of 10 cm focal distance as a receiver and transmitter pair. The transducers were aligned along a common axis 20 cm apart from each other in a water tank. A pulse generator (Systron Donner 101, Walnut Creek, USA) was used to excite the transmitting transducer. Each sample was placed at the focus of the two transducers and the ultrasound pressure wave after propagation was received and converted to a digital signal by the receiving transducer which was then displayed on an oscilloscope (Tek TDS 5052, Beaverton, USA). To eliminate the reflection losses from the faces of the specimen and to establish the attenuation-frequency relationship, the acoustic attenuation through two of the phantoms was used in the following equation in which P_2 and P_1 refer to the attenuated pressure wave amplitudes through the

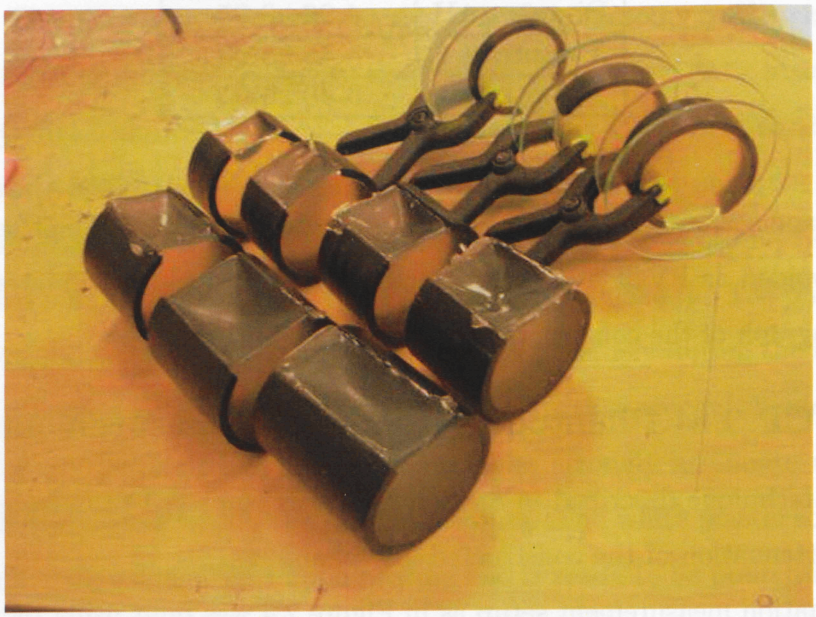

Figure 2.3: A set of 10 PVCP tissue-mimicking phantoms, which corresponds to the phantoms listed in table 2.1

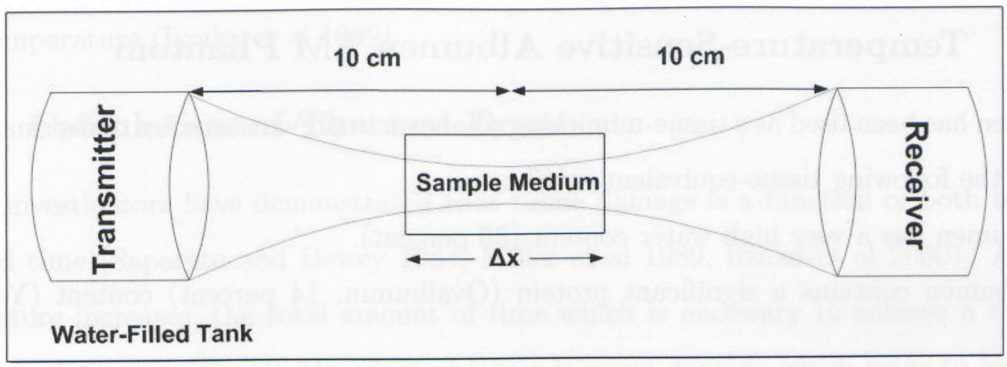

(a) Schematic of acoustic attenuation measurement setup

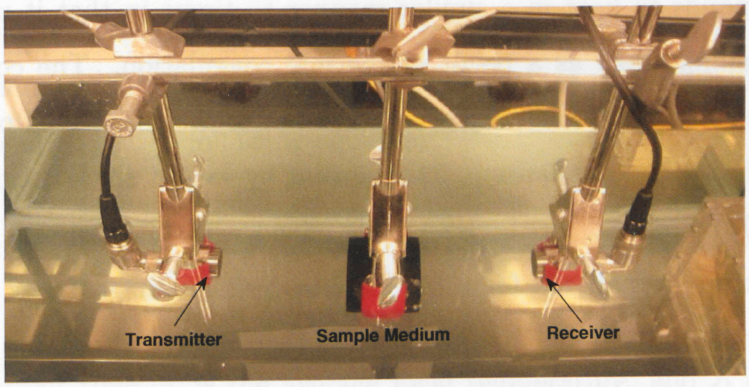

(b) Acoustic attenuation measurement setup

Figure 2.4: Acoustic Attenuation Measurement Setup

longer and shorter phantoms, respectively. Δx indicates the thickness difference between the two phantoms. The attenuation coefficient can then be calculated by:

$$\alpha_{dB} = \frac{-20}{\Delta x} log_{10} \frac{P_2}{P_1} \tag{2.1}$$

The measurement was repeated for five times on the same phantom in a frequency range of 3.5-7.5 MHz at discrete intervals of 0.5 MHz.

2.2 Heating Experiments

2.2.1 Temperature-Sensitive Albumen TM Phantom

Albumen has been used as s tissue-mimicking phantom in previous studies of thermal damage due to the following tissue-equivalent attributes:

1. Albumen has a very high water content (86 percent).
2. Albumen contains a significant protein (Ovalbumin, 14 percent) content (Yang et al 1991).
3. The albumen phantom is essentially a homogeneous medium.
4. Albumen is easily available and reproducible.
5. Albumen responds to heat in a similar manner to tissue in that it undergoes a visible irreversible whitening effect as a result of thermal coagulation. The coagulated albumen appears white in room light, facilitating visualization of the coagulated phantom regions.

To prepare the Albumen phantom, 22.2 percent by weight chicken egg albumen powder (Crude, Grade II, Sigma, St. Louis, USA) was mixed with 77.8 percent by weight distilled water. This mixture was stirred for a few minutes using a magnet bar until the albumen powder was dissolved in water. The mixture was then filtered through a fine-mesh sieve to produce a yellow, homogeneous albumen stock solution. 13.3 percent by weight of a dye stock prepared by dissolving 0.387(g) Naphthol Green Dye (Sigma) in 1L distilled water was mixed with 32 percent by weight distilled water. As the mixture reached 70 °C, 1.5 percent by weight of agar powder (Agar ♯1, Oxoid, Hampshire, England) was added to the heated dye stock and dissolved until the boiling point (85°C) was reached. The agar and dye mixture was removed from the hot plate and cooled to 45°C to prevent albumen coagulation on contact. At the same time, 53.3 percent by weight of the prepared albumen stock was warmed in a circulating water bath to 40°C to avoid uneven gelling and bubble formation within the agar solution. The albumen was then added to the dye-agar solution and stirred gently. This mixture was poured into 2-cm PVC piping shaped molds through the hole which was drilled on the side of the mold. The phantom was then let cool and solidify for

approximately 2 hours which is the time it takes until the albumen phantom reaches the room temperature (Iizuka et al 1999).

2.2.2 Calculation of Thermal Dose

Several investigators have demonstrated that tissue damage is a function of both temperature and time (Sapareto and Dewey 1984, Miller et al 1989, Iizuka et al 2000). As tissue temperature increases, the total amount of time which is necessary to achieve a threshold of damage decreases. The development of tissue thermal damage which leads to lesion formation in thermal therapy can be defined best by thermal dose criterion which links the temperature achieved and the time of exposure in a nonlinear fashion. The concept of "cumulative equivalent minutes" is a mathematical model which is based on the thermal dose received after 1 hour at 43 °C, and is sufficient to be lethal to tissue. This mathematical model can be explained by the following equation:

$$t_{43} = \sum_{t=0}^{t=final} R^{43-\overline{T}} \triangle t \tag{2.2}$$

where t is the current time, $\overline{T}$ is the average local temperature, and R is 0.5 for temperatures above 43 °C and 0.25 for temperatures below 43 °C (Sapareto and Dewey 1984). Tissue is usually non-homogeneous in its structure at multiple scales. This could be one reason as to why non-uniform temperature distribution in solid tumours during a thermal therapy treatment happens. Methods based on thermal dose measurement describe these temperature non-uniformities, taking time and temperature into account. Thermal dose for albumen heating was calculated based on temperature measurements of albumen samples of 2 cm thickness which were made following the recipe described in Section 2.2.1. For the water bath heating, the albumen phantom was clamped between two pieces of glass, so that the albumen sample is not in contact with the hot water. A screw was used to cover the hole on the mold and a needle-type thermocouple (Omega, HH306, CT) was inserted into the center of the albumen phantom through a small hole drilled into the screw as shown in

Figure 2.5 to record the temperature profile during heating to 70 °C and cooling to the room temperature.

Each albumen phantom was imaged prior to and after being heated for different time

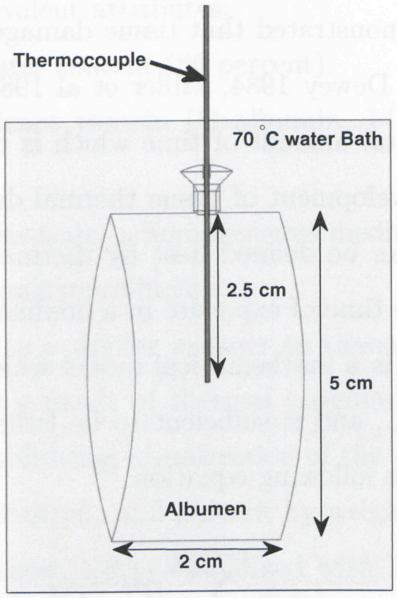

Figure 2.5: The schematic of albumen heating experimental apparatus.

intervals inside the 70°C circulating water bath. A waiting time of 30 minutes inside AcoustoCam's water tank before image acquisition ensured that the heated albumen had reached the room temperature. After reaching the room temperature, each phantom was imaged by the AcoustoCam setup. The corresponding attenuation value for each sample was obtained by acquiring the 8-bit and the uncompressed 14-bit mean pixel intensities and using the mean pixel intensity-attenuation relation.

2.3 Laser Heating Experiments

Laser interstitial Thermal Therapy (LITT) describes the direct thermal destruction of tumour cells using laser energy. LITT uses low energy (3-20 Watts) laser light in continuous

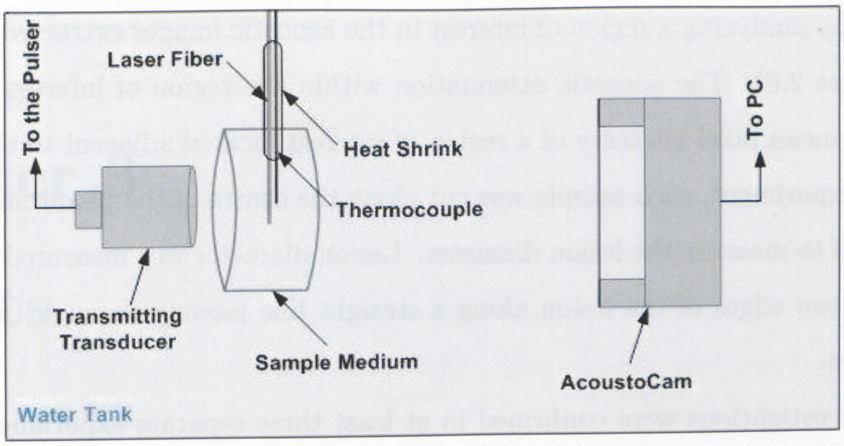

Figure 2.6: Schematic of the laser heating setup. A video stream was acquired during the laser heating experiment at a recording rate of 30 frames per second.

mode applied over 2-20 minutes. Slow heating prevents carbonization and vaporization of the tissue regions next to the laser fiber. Due to laser light energy absorption by the tissue, high temperatures that exceed 55 °C are produced locally in the target tissue. This leads to an irreversible protein coagulation and destruction of diseased tissue cells.
The proposed methodology in this study was validated in two sets of experiments with albumen tissue mimicking phantoms and ex-vivo liver tissue slabs. The laser applicator which was a 2-cm cylindrical diffuser with a core diameter of 800 micrometers (Photoglow, Yarmouth, MA) was used to induce high temperatures in regions surrounding the laser fiber, leading to localized protein coagulation.

In each experiment, a needle-type thermocouple was inserted into the sample along with the laser fiber with the measuring tip placed in the middle of the light-emitting portion of the light diffuser to measure the temperature variations close to the laser applicator. The temperature profile in each heating experiment was used to calculate the received thermal dose during the experiment and correlate this to the attenuation changes measured.

A video stream was acquired at a rate of 30 frames per second of prior, during and

after each laser heating experiment. The effect of heating on attenuation of each sample was investigated by analyzing a region of interest in the acoustic images extracted from the video stream (Figure 2.6). The acoustic attenuation within the region of interest was calculated based on the mean pixel intensity of a region of interest located adjacent to the probe. After the heating experiment, each sample was cut along the centre of the phantom to photograph the lesion and to measure the lesion diameter. Lesion diameter was measured as the distance between the two edges of the lesion along a straight line passing through the center of the thermal lesion.

All the investigations were confirmed in at least three separate experiments and the average of the experiments were used as the final assessment of the heating effect on acoustic attenuation. The measurement variability was estimated by calculating the standard deviation of the experimental values obtained.

Chapter 3

Results

3.1 AcoustoCam's Calibration

Prior to using the AcoustoCam to investigate the effects of thermal therapy, a set of tissue-mimicking phantoms with thickness values as listed in Table 2.1 were constructed and the acoustic attenuation for each phantom was measured employing an insertion technique (Section 1.5.1). The phantoms were imaged using the AcoustoCam setup to establish a relationship between the measured mean pixel intensities of the acoustic images to the known attenuation values of the constructed phantoms.

Figures 3.1(a) and 3.1(b) show acoustic attenuation measurements for the phantoms between 3.5 MHz and 7.5 MHz. The attenuation measurement was repeated in five different experiments. These five measurements were averaged and the averaged value was graphed against the corresponding frequency. The standard deviation was calculated over five sets of measurement at each frequency interval to demonstrate the experiment reproducibility. The small error bars on each graph show the precision of the measurement.

One concern with the measurements made were the losses that may occur due to reflection off the phantom surface. The attenuation at each frequency interval was calculated using the attenuated pressure wave through phantoms D and E and normalizing it by the thickness difference between the two phantoms. Figure 3.2 shows the calculated attenuation graphed against each frequency interval and fitted to a power law equation.

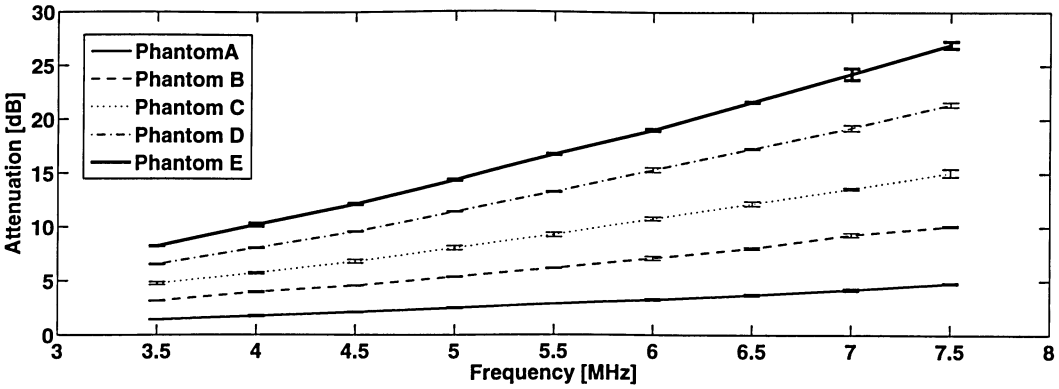

(a) Acoustic Attenuation Change with frequency for phantoms A, B, C, D, E

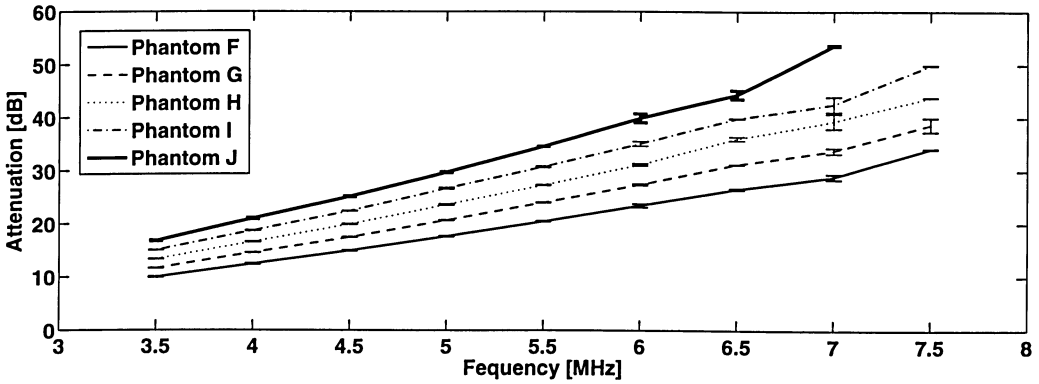

(b) Acoustic attenuation change with frequency for phantoms F, G, H, I, J

Figure 3.1: A broadband insertion technique was employed to measure the ultrasonic attenuation of a set of PVCP tissue-mimicking phantoms for the whole frequency range of 3.5 MHz to 7.5 MHz. The figures show graphs of acoustic attenuation versus frequency for phantoms labeled (a) A, B, C, D, E and (b) F, G, H, I, J. The error bars represent the standard deviation for conducting the experiment five times. Phantom labels have been adopted from table 2.1.

Fitting the attenuation-frequency dependence to a power law, the following equation was obtained through which the attenuation coefficient could be calculated at each frequency (in units of dB/cm):

$$\alpha = (0.38 \pm 0.05) f^{(1.54 \pm 0.12)} \tag{3.1}$$

The attenuation values for the TM phantom set were re-calculated at each frequency interval using Equation 3.1 (table 3.1).

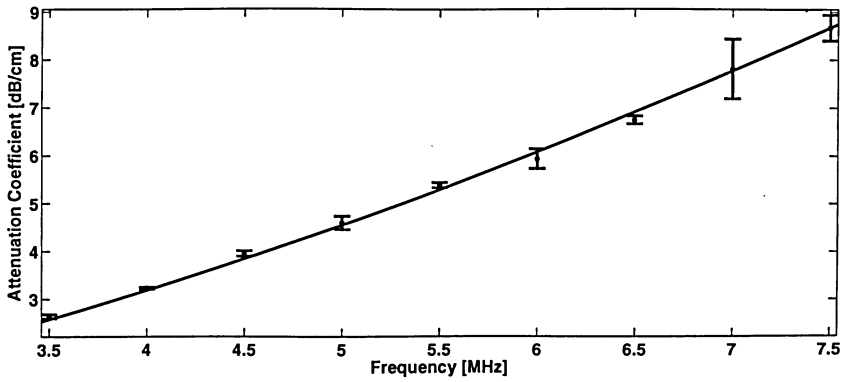

Figure 3.2: A graph of attenuation coefficient versus frequency calculated for Phantom E relative to Phantom D.

Figure 3.3 shows the small discrepancy between the ultrasonic attenuation with and without the reflection loss for each PVCP TM phantom. It also shows that attenuation is overestimated when the reflection loss is not eliminated.

Table 3.1: Acoustic attenuation of the PVCP phantom set at a frequency of 4.76 MHz.

Phantom	Thickness (cm)	Acoustic Attenuation (dB@4.76MHz)
Phantom A	0.52 ±0.05	2.18 ±0.03
Phantom B	1.17 ±0.05	4.91 ±0.04
Phantom C	1.71 ±0.05	7.18 ±0.20
Phantom D	2.42 ±0.05	10.16 ±0.05
Phantom E	3.17 ±0.05	13.31 ±0.06
Phantom F	3.72 ±0.05	15.62 ±0.06
Phantom G	4.30 ±0.05	18.06 ±0.06
Phantom H	4.93 ±0.05	20.70 ±0.09
Phantom I	5.45 ±0.05	22.90 ±0.13
Phantom J	6.30 ±0.05	26.46 ±0.09

3.1.1 AcoustoCam's Preparation for Acoustic Imaging Purpose

Prior to operating the AcoustoCam setup for imaging purposes, the AcoustoVision software was used to adjust parameters for an optimized attenuation dynamic range within the at-

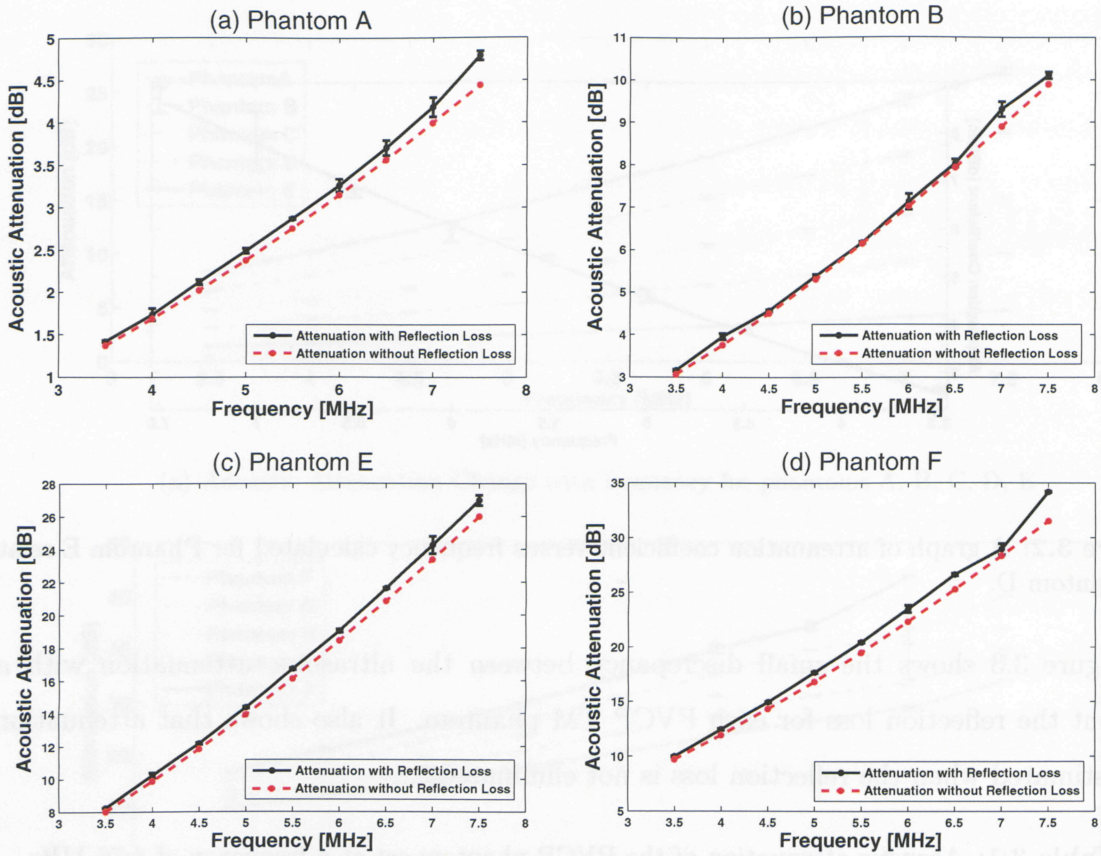

Figure 3.3: Acoustic attenuation measurement for PVCP phantoms A, B, E and F. An insertion technique was employed to measure the ultrasonic attenuation of each phantom for frequencies ranging from 3.5 MHz to 7.5 MHz.

tenuation range of 26.46 dB at 4.76 MHz:

Dynamic Range Correction

The first step involved optimizing the dynamic range of the camera for the highest and lowest attenuation for these experiments. This was done by acquiring the 14-bit data through the water-only path and through the thickest PVCP phantom (highest attenuation value). The upper level of the dynamic range correlated with the water-only path was set to 7900 and the lower limit of the dynamic range related to imaging the thickest PVCP phantom was set to 3000. This resulted in an increased dynamic range by truncating the unused portions of

the uncorrected display.

Delay Distance

The delay distance is based on the length of the water path from the transducer to the detector. It specifies the length of time at which the detector is active (assuming an ultrasound velocity of 1500 m/s). The fixed distance between the outermost acoustic lens and the detector in the AcoustoCam setup is 8.6 cm. For an object placed 12.5 cm away from the outermost lens with the illuminating transducer directly behind the object, a distance of 180 cm or 120μs is optimal.

Image Saturation

During imaging, image saturation should be avoided so that the available image data is used to its full extent. The full range between when the pulser is off and when the pulser is being used at its maximum intensity is divided into 126 levels. In order to make sure that no saturation in the image occurs, the pulser amplitude was increased and the corresponding 8-bit and 14-bit mean pixel intensities were acquired at each intensity setting.

Figure 3.4 shows how the 8-bit and 14-bit mean pixel intensities change for different settings of the pulser amplitude. The image saturation for the 8-bit data or the image display occurred after an amplitude control (AC) level of 41. No image saturation was detected for the 14-bit sensor's output. This shows the greater dynamic range of the 14-bit AcoustoCam's output and that the AC level of 41 is suitable for both 8-bit and 14-bit data acquisition process.

Image Size

This step was performed in order to approximate the image size and relate the number of the pixels in the image to the actual size of the object being scanned. For the fixed distance settings used in this experiment, a metal grating and a Canadian dime were imaged in the AcoustoCam setup.

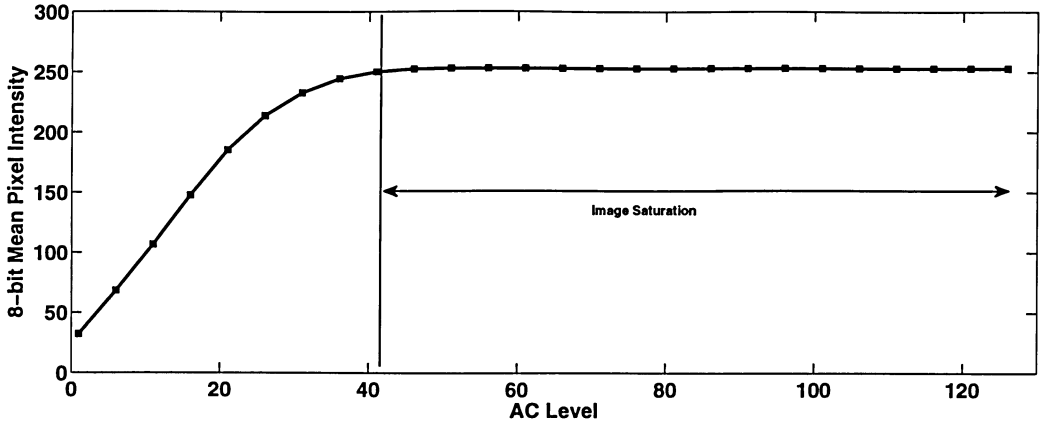

(a) 8-bit image intensity as a function of amplitude control

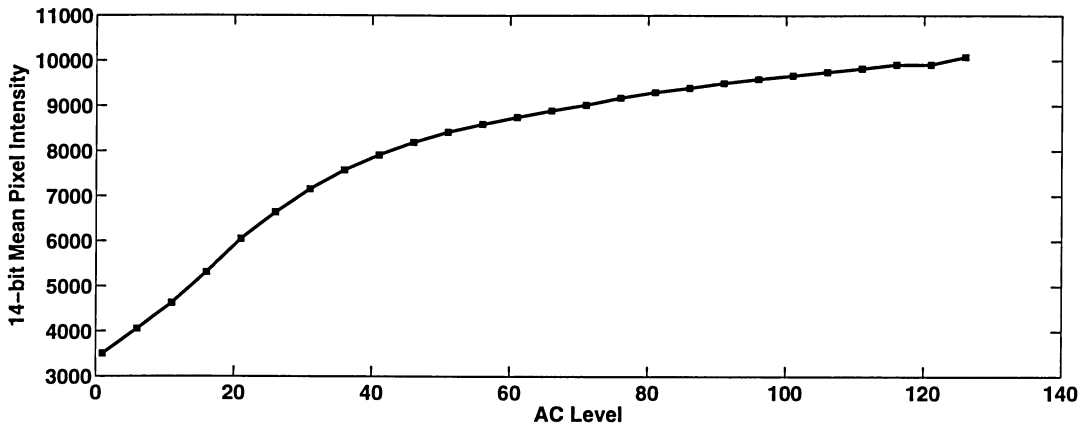

(b) 14-bit image intensity as a function of amplitude control

Figure 3.4: 8-bit and 14-bit mean pixel intensity variation with AcoustoCam amplitude settings (AC level) increased to determine the saturation level in the transmission ultrasound images.

It was calculated that each pixel in the image corresponds to 0.13±0.01 mm.The acoustic images are shown in figure 3.5.

3.1.2 Transmission Ultrasound Imaging of the PVCP Tissue Mimicking Phantom Set

The PVCP TM phantoms were imaged in the AcoustoCam setup to establish a relationship between acoustic attenuation and mean pixel intensity. A phantom holder was used to place each phantom between the transmitting transducer and the receiving part of the Acousto-

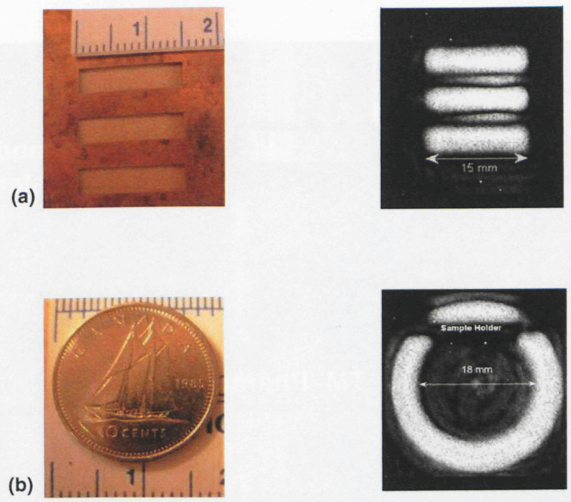

Figure 3.5: Transmission ultrasound images of a (a) metal grating whose grating was 15 mm×3 mm and (b) Canadian dime (diameter 18.03 mm)

Cam as shown in Figure 3.6.

The AcoustoCam setup was used to image each tissue-mimicking phantom. The acquired acoustic images are grayscale images with pixel intensities ranging from 11 to 248 which allows 237 levels of intensity (i.e. shades of gray). The results shown in Figure 3.7, clearly demonstrate that the higher the attenuation value, the darker the acoustic image pixel intensities are.

As previously described, two types of data could be extracted from the AcoustoCam setup. The Matlab image processing package was used to obtain the 8-bit image data displayed on the monitor. 14-bit mean pixel intensities were extracted using the AcoustoVision software. The higher the ultrasonic attenuation, the lower the mean pixel intensities are. Hence, the image will appear as darker to the viewer. Both the 8-bit and 14-bit mean pixel intensities were graphed against their corresponding attenuation values as illustrated in Figure 3.8.

Now that the AcoustoCam is calibrated with a set of phantoms with know attenuation values, it is ready to be used to investigate the effect of heating on attenuation attributes of

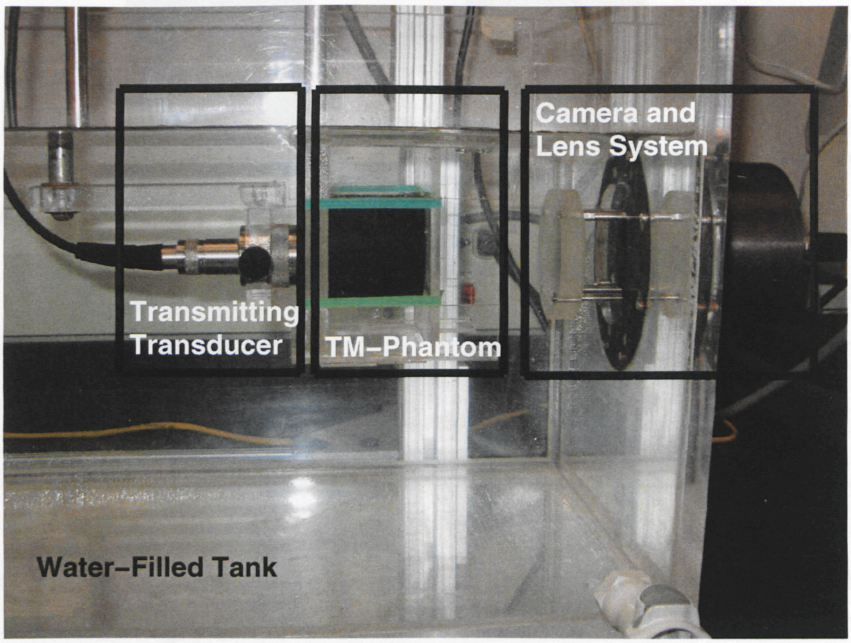

Figure 3.6: The AcoustoCam imaging setup.

temperature sensitive samples.

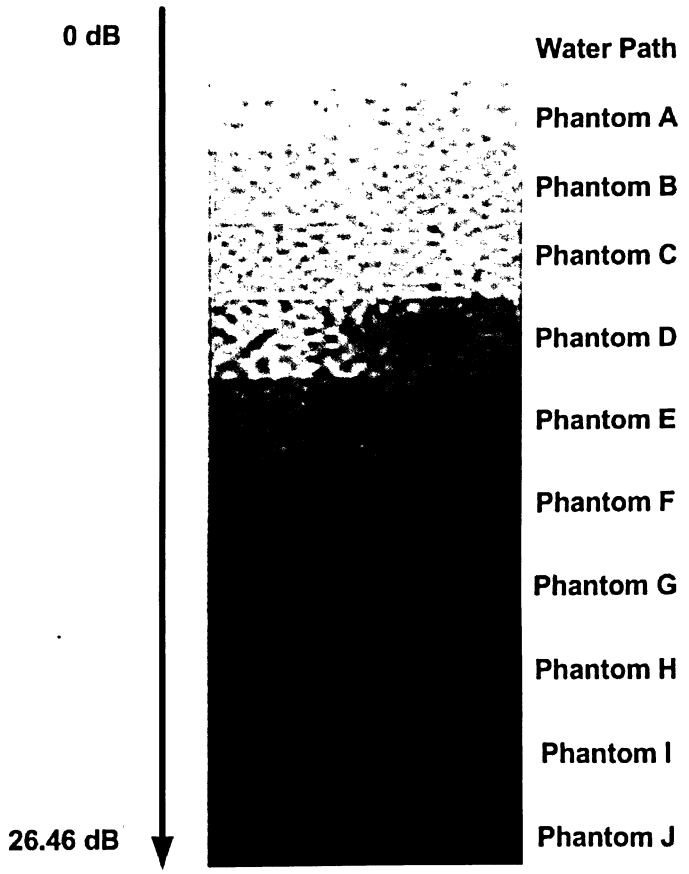

Figure 3.7: Transmission ultrasound images of the PVCP TM phantoms. The acoustic images cover an ultrasonic attenuation range from 0 dB to 26.46 dB.

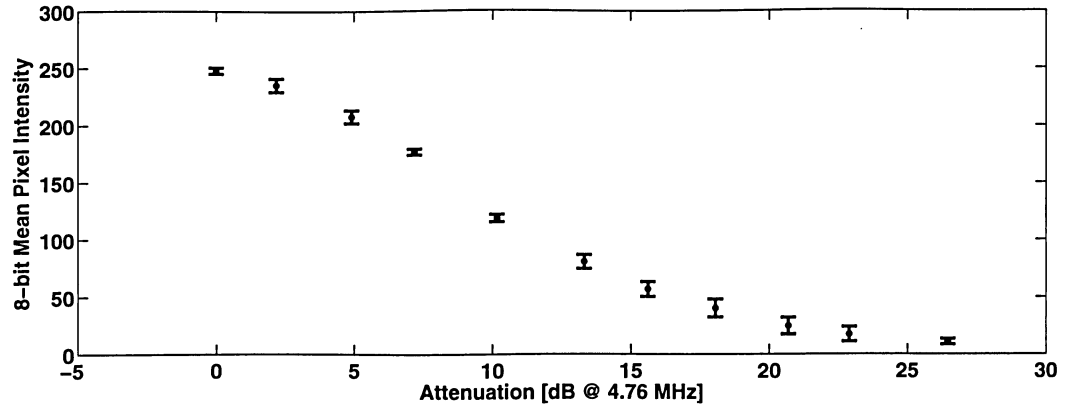

(a) 8-bit mean pixel intensity versus acoustic attenuation

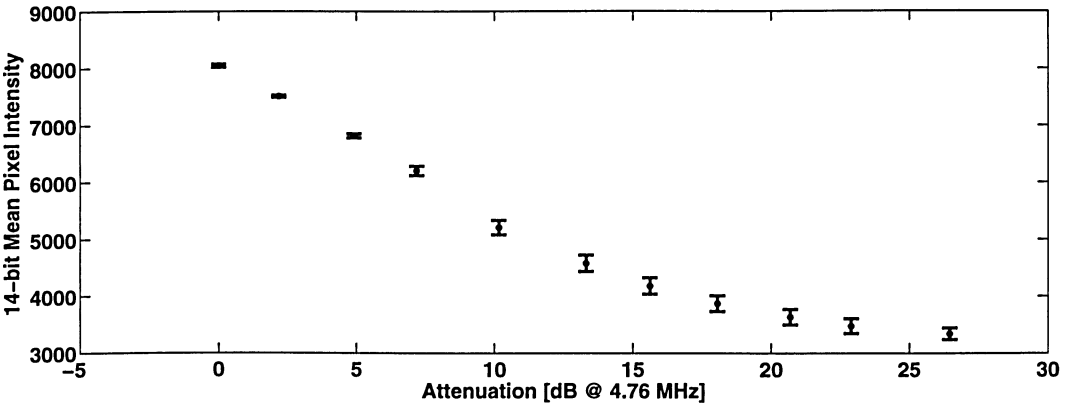

(b) 14-bit mean pixel intensity versus acoustic attenuation

Figure 3.8: 14-bit and 8-bit mean pixel intensities obtained from the AcoustoCam setup graphed against acoustic attenuation.

3.2 Heating Experiments

3.2.1 Thermal Dose Estimation for Albumen Heating

Figure 3.9 shows the average temperature profile of the albumen phantom during heating inside a 70 °C circulating water bath and cooling to room temperature and the resultant standard deviation based on performing three sets of the same experiment. It was shown that an average time amount of nearly 25 minutes was necessary for the center part of the albumen phantom to reach 70 °C. The temperature profile shown in Figure 3.9 was used to

calculate the thermal dose received after any required amount of time.

The next step was to determine the thermal dose threshold needed to cause thermal

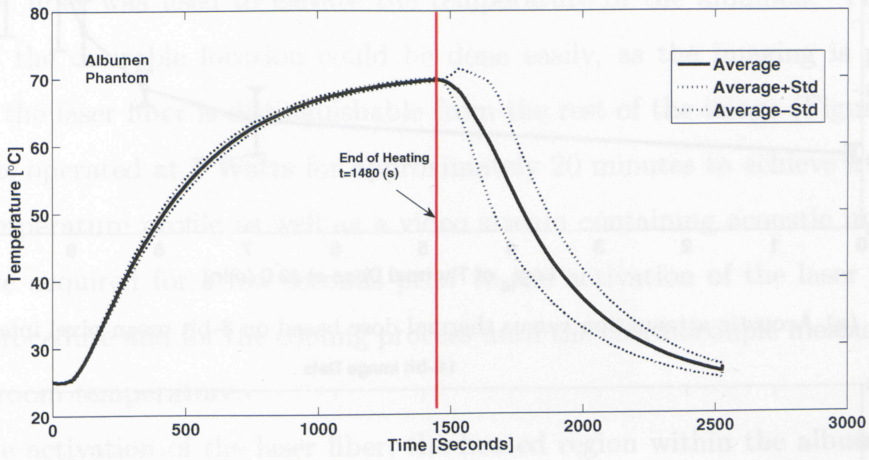

Figure 3.9: Average temperature profile at the center of albumen phantom for 70 °C water bath heating followed by cooling inside water at room temperature. The standard deviation as a result of repeating the albumen heating and cooling procedures in three separate experiments has also been graphed.

coagulation based on the acoustic attenuation obtained with the AcoustoCam system.

The fractional change in acoustic attenuation was used to quantify the influence of thermal dose on ultrasonic attenuation and to specify the thermal dose threshold for a complete thermal coagulation:

$$att_{change} = (\alpha_{heated} - \alpha_{unheated})/\alpha_{unheated} \tag{3.2}$$

Figure 3.10 shows the fractional change in attenuation for each received thermal dose. It is known that when thermal dose reaches the threshold for protein coagulation, tissue attenuation increases. The attenuation of soft tissue has shown to increase at dosages in the range of 100-1000 minutes (with the thermal dose referenced to 43°C) (Damianou et al 1997). A similar process occurs in the albumen phantoms. In the albumen experiments, an increase in attenuation was observed at doses higher than 7.86×10^6 min (referenced at 43 °C), with the maximum attenuation reached at 1.37×10^9 min (in equivalent minutes referenced at 43 °C). This equilibrium state was achieved at exposure times longer than 1800 seconds.

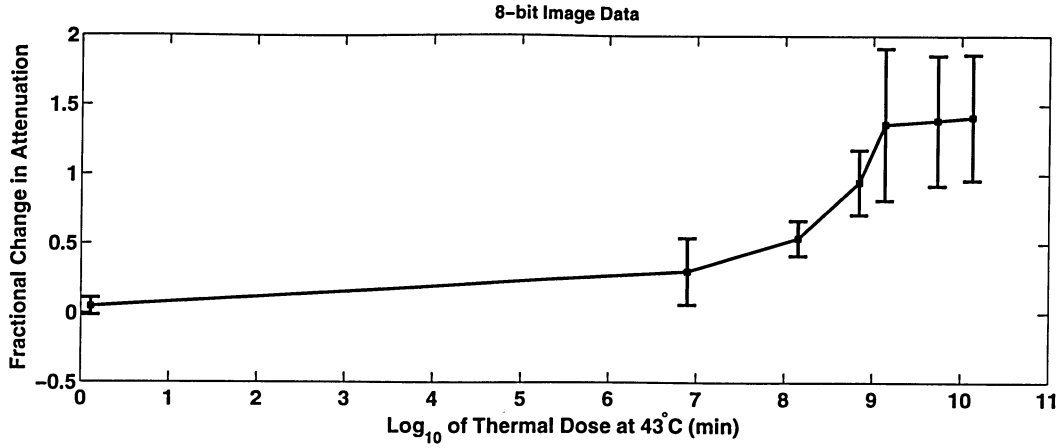

(a) Acoustic attenuation versus thermal dose based on 8-bit mean pixel intensity

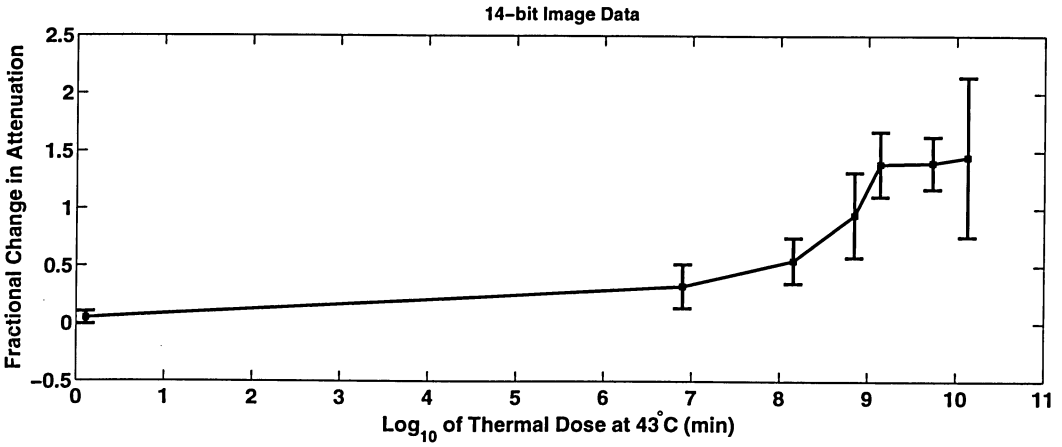

(b) Acoustic attenuation versus thermal dose based on 14-bit mean pixel intensity

Figure 3.10: Thermal dose calculation based on 8-bit and 14-bit data acquisition with the AcoustoCam. The error bars are the result of repeating the experiment for three times.

This means that after receiving a thermal dose of 1.37×10^9 min (in equivalent minutes referenced at 43 °C), total coagulation has occurred, because receiving higher thermal doses does not further increase the acoustic attenuation and the fractional change in attenuation remains at 1.4. Moreover, the irreversibility of the attenuation changes in albumen shows that these attenuation changes depend on the structural changes in the albumen, and not on temperature.

3.2.2 Albumen Laser Heating

2-cm thick albumen phantoms were prepared according to the recipe presented in Section 2.2.1. A laser fiber was used to elevate the temperature of the albumen. The applicator placement at the desirable location could be done easily, as the imaging is performed in realtime and the laser fiber is distinguishable from the rest of the image (Figure 3.11). The laser fiber was operated at 7 Watts for approximately 20 minutes to achieve a slow heating rate. The temperature profile as well as a video stream containing acoustic images of each phantom were acquired for a few seconds prior to the activation of the laser fiber, during the heating procedure and for the cooling process until the thermocouple measured the same value as the room temperature.

Upon the activation of the laser fiber, the heated region within the albumen phantom

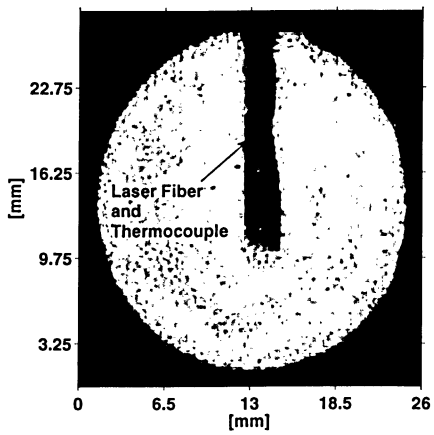

Figure 3.11: Albumen phantom acoustic image showing the inserted laser fiber and thermocouple probe.

became brighter in the acoustic attenuation measurements. This effect is hypothesized to be the result of the decrease of acoustic attenuation of water with increasing temperature, as water is the greatest constituent of the albumen phantom used in this study. After the heating experiment, each albumen phantom was sectioned and photographed and the diameter of the lesion was measured.

Figure 3.12 shows the created thermal lesion which is in the shape of an ellipsoid. This

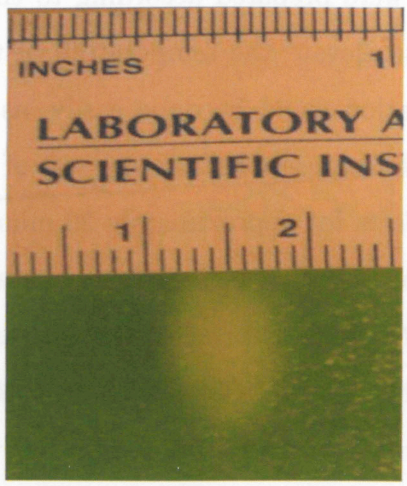

Figure 3.12: Laser heating creates a thermal lesion within an albumen phantom. The thermal lesion is apparent on the photograph as a white ellipsoidal region which is created due to the increased scattering in the phantom.

is the shape expected for laser heating with a diffusing fiber tip. It is also evident that high temperatures lead to a visible whitening effect within albumen as a result of thermal coagulation.

Figure 3.13 shows the estimated lesion boundary on an acoustic image recorded during the heating experiment. The lesion boundary selection on the image was based on a lesion diameter of 0.72 cm.

A sequence of acoustic images taken during the laser heating procedure has been shown in Figure 3.15. The heated regions could be seen brighter on the acoustic images. The images extracted from the recorded video stream were used to see how attenuation changes during the heating experiment. The region of interest on the acoustic images was selected such that it is located inside where the lesion was expected to be created. This is done by specifying the boundaries of the lesion on the acoustic images assuming a lesion diameter size of approximately 0.72 cm.

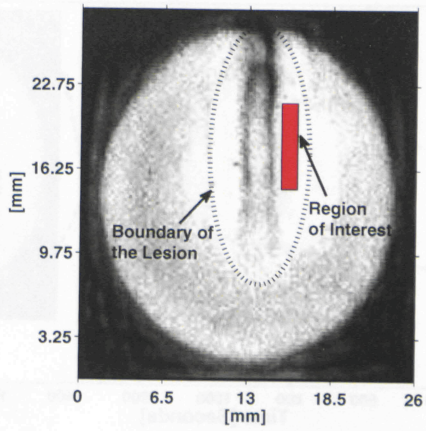

Figure 3.13: The lesion boundary is specified on an acoustic image taken during a laser heating experiment. This facilitates the selection of a region of interest within the thermal lesion.

Real-time transmission ultrasound imaging performed using the AcoustoCam, detected an initial rapid decrease in attenuation, followed by a gradual attenuation increase.

The graphs shown in Figure 3.14 are the result of extracting images from the acquired video stream every two seconds and finding the mean pixel intensities in the region of interest (Figure 3.13) and calculating the corresponding attenuation values.

After turning off the laser power, acoustic attenuation continued to increase at a faster rate. The attenuation changes as a function of time are shown in Figure 3.14 for three different laser heating experiments.

The water heating effect tends to cause a decrease in attenuation, with the greatest decrease in the temperature range of 20-50 °C (Figure 1.8). This is a reversible effect, as can be seen by the rapid increase in attenuation that occurs when laser is turned off. Changes of acoustic attenuation during periods of heating and cooling could therefore be categorized into three clearly distinct stages:

Stage 1. The initial steep decrease in attenuation which is hypothesized to be related to the temperature dependence of water attenuation.

Stage 2. The gradual increase in attenuation after the temperature at which coagulation

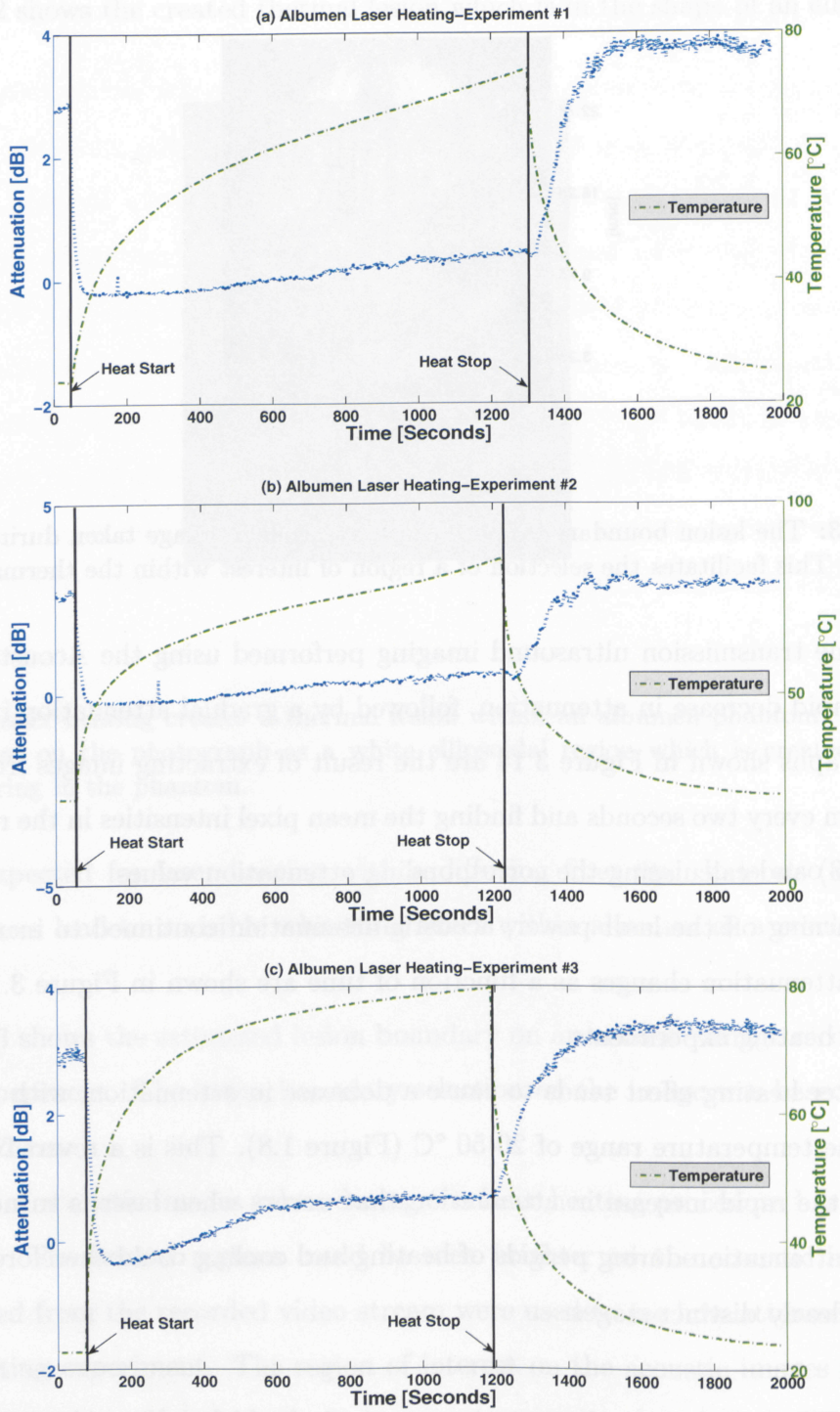

Figure 3.14: Plot of the changes in acoustic attenuation and temperature 1. prior to heating 2. heating for 20 minutes and 3. cooling to room temperature (demarcated by the vertical bold lines). Figures a, b and c show the experimental data for three different experiments with albumen.

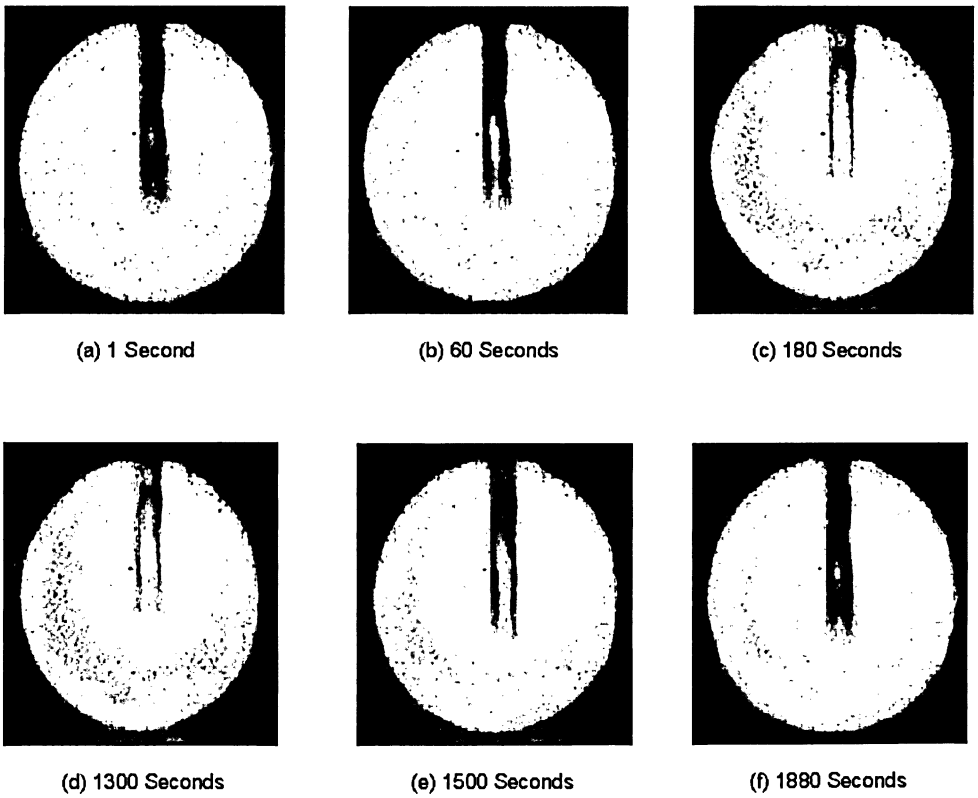

Figure 3.15: Sequence of acoustic images during heating of the albumen phantom. Heating was turned off at 1300 seconds.

occurs is reached.

Stage 3. The final rapid increase in attenuation after the heating.

The result of averaging the experimental attenuation measurements is shown in Figure 3.16. The resultant standard deviation has also been graphed as a function of time and shows a small dispersion from the mean attenuation value which shows the very good experiment reproducibility.

Table 3.2 summarizes the findings on attenuation and temperature variations at different stages of the heating experiments.

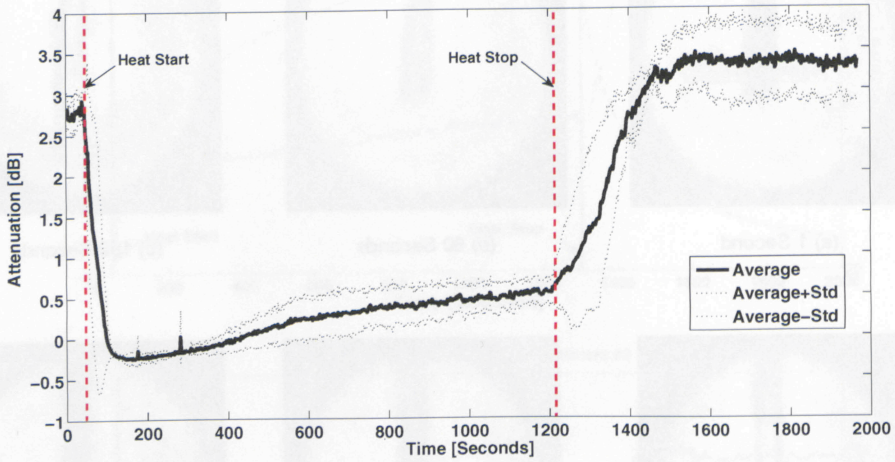

Figure 3.16: The average attenuation value as a result of conducting the albumen laser heating procedure in three different experiments has been graphed as a function of time. The resultant standard deviation shows a small dispersion from the average attenuation value.

Table 3.2: An overview of findings during albumen laser heating in three different experiments.

Variable	Experiment♯1	Experiment♯2	Experiment♯3	Average
Initial Attenuation Decrease (dB)	2.96	2.8	3.28	3.00
Total Attenuation Increase (dB)	0.96	0.26	0.42	0.52
Received Thermal Dose (min at 43 °C)	3.05×10^{09}	5.38×10^{12}	3.93×10^{11}	1.92×10^{12}
Lesion Size (cm)	0.75	0.70	0.71	0.72
Temperature Range (°C)	23.8-74.1	22.7-85.5	22.8-79.7	23.1-79.76

3.2.3 Ex-vivo Laser Heating Experiments

The dynamics of the attenuation behaviour of biological tissue during laser heating was studied in tissue samples of bovine liver. Bovine liver tissue was bought from a local grocery store and kept out of fridge until the temperature of the liver reached the room temperature. Each liver specimen was placed inside the sample holder for the heating experiment. Liver tissue has a greater optical absorption compared to albumen. Therefore, the power at

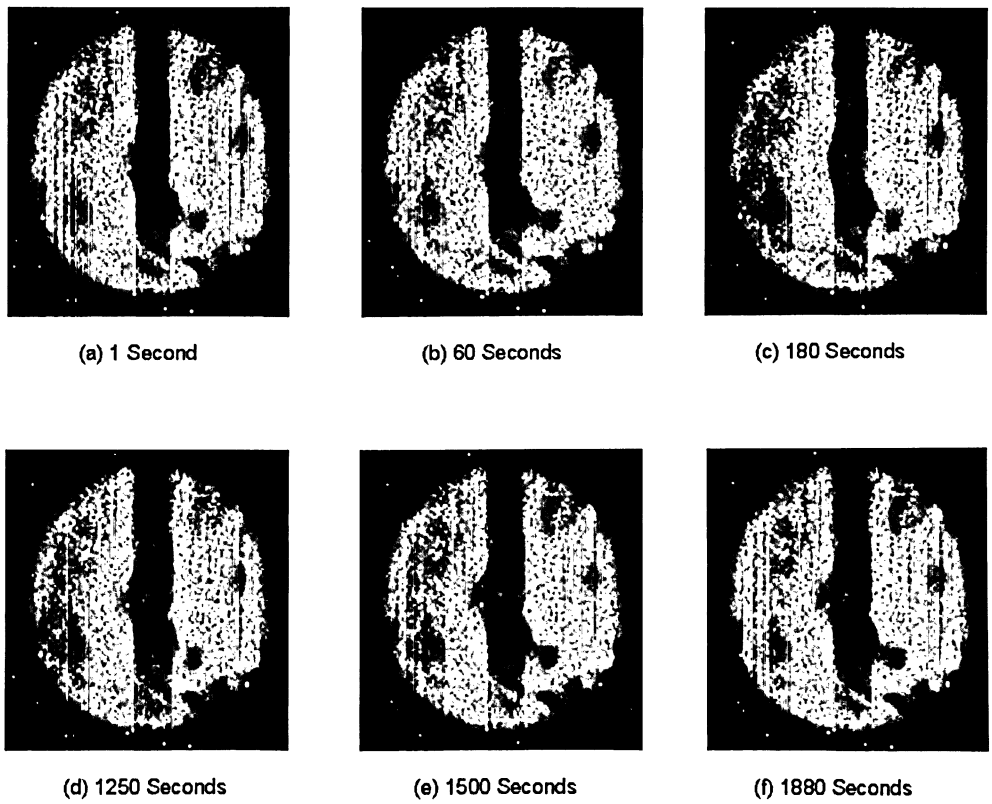

Figure 3.17: A sequence of acoustic images of bovine liver taken during a laser heating experiments. These images were used to assess the effect of heat on the acoustic attenuation.

which laser was operated was reduced to 4 Watts to avoid charring. Thermal lesions were created in four different liver slices. Video recording was performed before, during and after

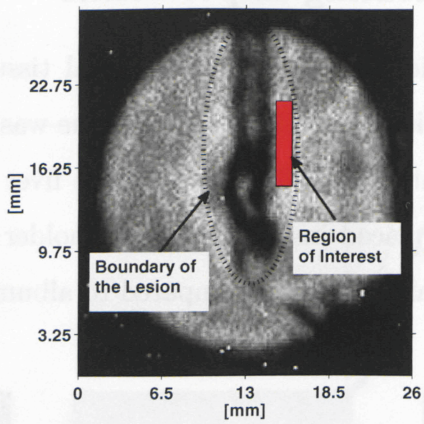

Figure 3.18: The boundary of the created thermal lesion within bovine liver tissue have been specified on an acoustic image taken during the experiment.

heating at a rate of 30 frames per second (Figure 3.17). The heated regions, however, were not as apparent on the acoustic images as they were for albumen laser heating experiments. The temperature was also measured for the above-mentioned periods every two seconds to investigate the effect of heating on the attenuation value of each tissue sample.

Figure 3.18 shows the thermal lesion boundaries on an acoustic image taken during the heating experiment, assuming a lesion size of approximately 0.71 cm. The purpose of specifying the lesion boundaries on the acoustic image was to make sure that the region of interest is selected within the area where the lesion was created.

After each heating experiment, the tissue was cut along the center of the thermal lesion. The exposed lesion was photographed and the radius of the thermal lesion was measured. The shape of the lesion created in this study is shown in Figure 3.19. Similar to the albumen heating experiments, the thermal lesion could be detected as an ellipsoidal white region with the bovine liver tissue.

Figure 3.20 shows the result of processing the mean pixel intensities (and therefore acoustic attenuation) within a region of interest specified in Figure 3.18 for four different laser heating experiments with bovine liver. The temperature history has also been graphed as a function of time.

The change in acoustic attenuation in a laser heating experiment follows the same trend as in the experiments conducted on the albumen phantoms (Figure 3.20).

Figure 3.21 is the result of averaging the attenuation values for the heating experiments

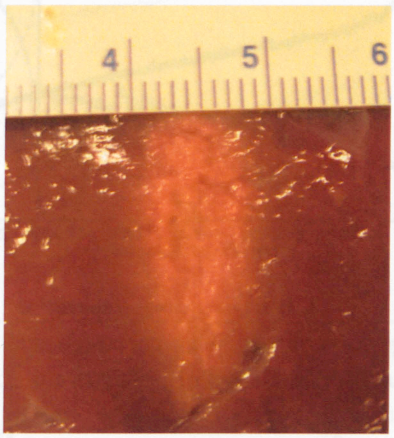

Figure 3.19: Photograph of a thermal lesion within a bovine liver sample. The lesion diameter is approximately 0.7 cm.

performed as a function of time. The standard deviation graph shows the variation around the mean attenuation value.

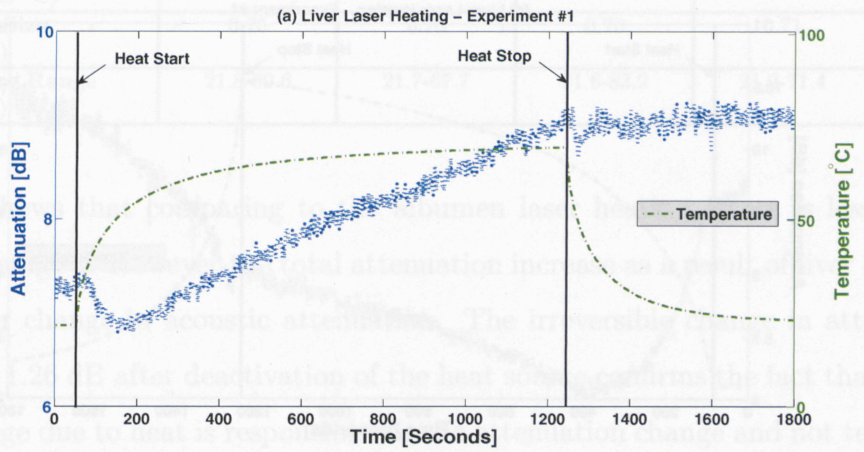

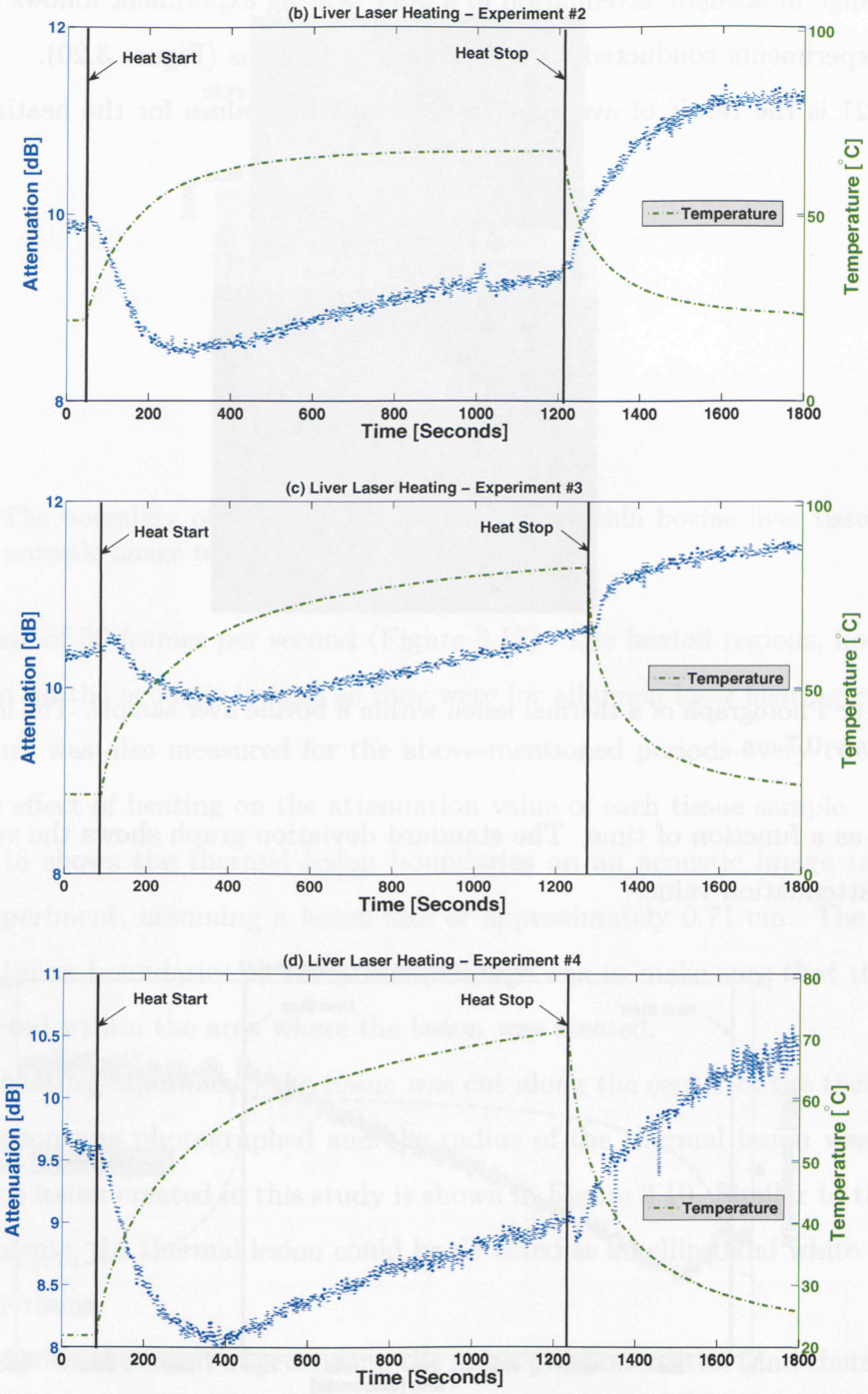

Figure 3.20: Plot of the changes in acoustic attenuation and temperature for 1. prior to heating 2. heating for 20 minutes and 3. cooling to room temperature (demarcated by bold vertical lines). Figures a, b and c show the experimental data for three different experiments with albumen.

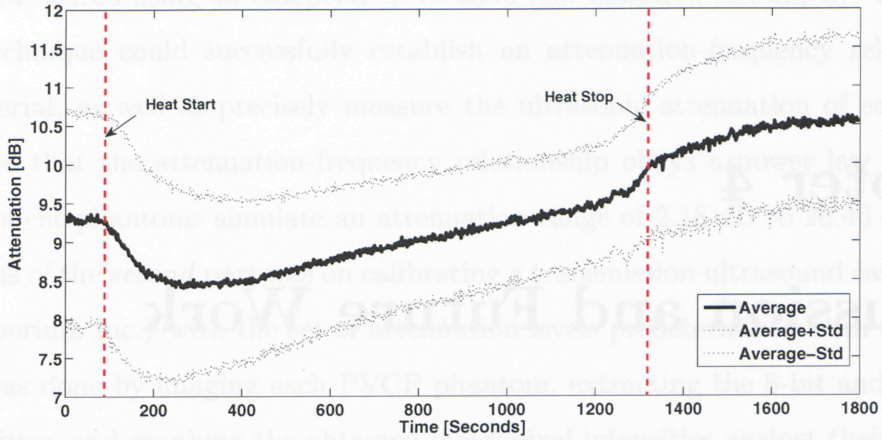

Figure 3.21: Plot of the average change in acoustic attenuation as a function of time. The average attenuation profile is the result of performing four different heating experiments on bovine liver samples. The standard deviation of the experiments has also been graphed as a function of time.

Table 3.3: An overview of findings during liver laser heating in four different experiments. Thickness of liver was approximately 2 *cm*.

Variable	Experiment♯1	Experiment♯2	Experiment♯3	Experiment♯4	Average
Initial Attenuation Decrease (dB)	0.47	1.37	0.55	1.62	1.00
Total Attenuation Increase (dB)	1.80	1.34	1.11	0.81	1.26
Received Thermal Dose (min at 43 °C)	5.48×10^{8}	2.16×10^{8}	3.7×10^{12}	8.48×10^{8}	9.25×10^{11}
Lesion Size (cm)	0.75	0.70	0.70	0.71	0.71
Temperature Range (°C)	21.8-69.6	21.7-67.7	21.6-83.2	21.9-71.4	21.75-72.97

Table 3.3 shows that comparing to the albumen laser heating, there is less change in attenuation in stage 1. However the total attenuation increase as a result of liver coagulation shows a greater change in acoustic attenuation. The irreversible change in attenuation of bovine liver by 1.26 dB after deactivation of the heat source confirms the fact that the tissue structural change due to heat is responsible for the attenuation change and not temperature.

Chapter 4

Discussion and Future Work

4.1 Discussion and Conclusions

The initial attenuation decrease for albumen occurs when the thermocouple inserted into the sample measured a temperature range of 23-65 °C. As the temperature increases beyond 65 °C, the attenuation starts to increase. The initial attenuation decrease for liver occurs when the thermocouple measures a higher temperature (27.3 °C) compared to the albumen laser heating experiments and ends at 60 °C which is lower than the temperature measured in albumen after the stage of the reversible attenuation decrease was over. The results presented in figure 3.19 are consistent with the fact that attenuation changes are greater and occur earlier for liver tissue as liver tissue is heterogeneous, has a greater light absorption and contains fat. Fat does not have much water and likely not as strong temperature dependence.

The irreversible increase in acoustic attenuation of tissue (or tissue-mimicking phantom) indicates that after passing the threshold for thermal damage the changes in attenuation are dependent on the structural changes within the sample and not on temperature.

This study ascertains the impact of thermal damage on acoustic attenuation through ex-vivo and tissue-mimicking phantom heating studies to provide quantitative estimates of acoustic attenuation during heating. The preceding chapters which demonstrate how acoustic attenuation could be used as an effective means of guiding a thermal therapy procedure comprised three parts.

In the *first* part PVCP tissue-mimicking phantoms were constructed and acoustic atten-

uation was measured using an independent method (the insertion technique). The employed insertion technique could successfully establish an attenuation-frequency relationship for PVCP material, as well as precisely measure the ultrasonic attenuation of each phantom. It was found that the attenuation-frequency relationship obeys a power law and that the tissue-equivalent phantoms simulate an attenuation range of 2.18 dB to 26.46 dB.

The focus of the *second* part was on calibrating a transmission ultrasound camera (AcoustoCam, Imperium Inc.) with the set of attenuation levels predetermined from the first step. This task was done by imaging each PVCP phantom, extracting the 8-bit and 14-bit mean pixel intensities, and graphing the obtained mean pixel intensities against their corresponding attenuation values. An important conclusion from this part was that the AcoustoCam could be used to estimate the attenuation value of a sample medium and proved to be sensitive to attenuation variations even at high attenuation values.

The established mean pixel intensity - attenuation relationship was used in the *third* part of this study to investigate the effect of heating on acoustic attenuation. The first step was to determine the time-temperature exposure (i.e. thermal dose) required for protein coagulation. Experimental results of albumen heating at 70 °C for different time exposures were correlated to the corresponding acoustic attenuation by using the mean pixel intensity. After receiving a thermal dose of 10^9 min (in equivalent minutes referenced at 43 °C), no significant increase in attenuation could be detected and the attenuation increased by a factor of 2.4. It could therefore be concluded that the complete coagulation of the sample had occurred by receiving this thermal dose. The results from the 14-bit mean pixel intensity correlates well with the 8-bit data and shows the same fractional change in attenuation. The temperature effect could not be observed in thermal dose estimation experiments, as the imaging process was performed after the albumen phantom reached room temperature.

The effect of laser heating was validated in temperature-sensitive phantoms and *ex vivo* bovine liver. The attenuation coefficient for albumen was found to be 1.40±0.05 dB/cm at 4.76 MHz. This value corresponds well with the albumen attenuation measurement which was done by the independent insertion technique in the lab. Laser heating was used to create

lesions which were ellipsoidal in shape and symmetric across the light-emitting portion of the laser fiber. The lesions were of predictable size and shape. To achieve predictable lesions too high an intensity or too long an exposure time must be avoided. Therefore, the laser applicator was operated at intensities below 7 Watts for no longer than 20 minutes to create lesions of approximately 0.7 cm diameter.

In the laser heating experiments with albumen phantoms and bovine liver tissue, the total attenuation of the region of interest was measured. Normalizing the total attenuation to the sample thickness only makes sense for a homogeneous sample medium. However, it is known that laser heating leads to the formation of a local thermal lesion within the sample. Therefore the resulting attenuation changes do not cover the whole sample and could not be normalized to the sample thickness. The total attenuation was obtained in the specified region of interests for laser heating experiments with albumen phantoms and bovine liver tissue. The results showed that laser heating caused an average attenuation increase of 0.54 dB and 1.26 dB in the albumen phantom and bovine liver tissue,respectively. Since the liver samples were measured to be approximately 2 cm, the attenuation coefficient of bovine liver was estimated to be 4.65±0.7 dB/cm. The diameter of the lesion was measured to be 0.7 cm and since the change in attenuation coefficient of 1.26 dB/cm was due to only the lesion, the total change in attenuation coefficient within the coagulated regions will be 1.75 dB/cm. This means that the attenuation coefficient for the coagulated parts of the liver is 6.3 dB/cm.

The average thermal dosages of 1.92×10^{11} (equivalents minutes at 43 °C) and 9.25×10^{11} (equivalent minutes at 43 °C) received for albumen and bovine liver respectively, correspond well with the thermal dose needed for a complete coagulation.

Temperature monitoring is one the most crucial components of any thermal therapy treatment. An interesting finding is that acoustic attenuation decreases with increasing temperature. However, after the sample cools down and reaches the room temperature, its attenuation value remains higher than before heating, suggesting that this attenuation increase is due to irreversible protein coagulation (Figure 4.1).

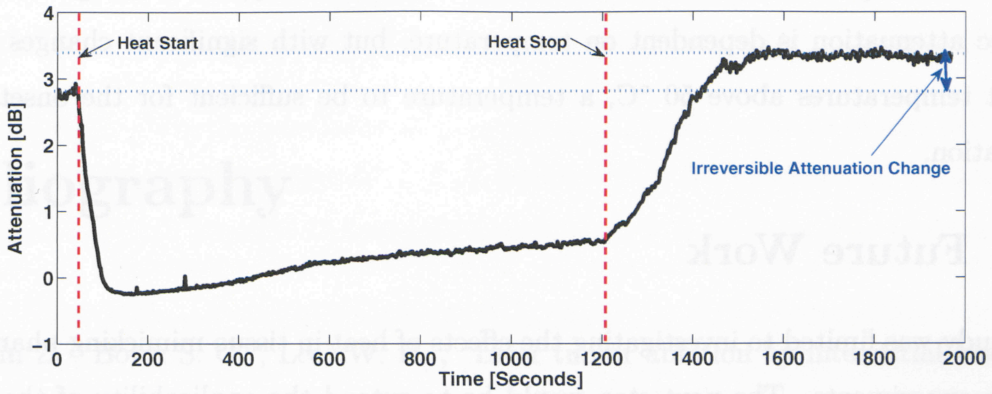

(a) The average attenuation change for albumen phantom as a result of performing three separate laser heating experiments.

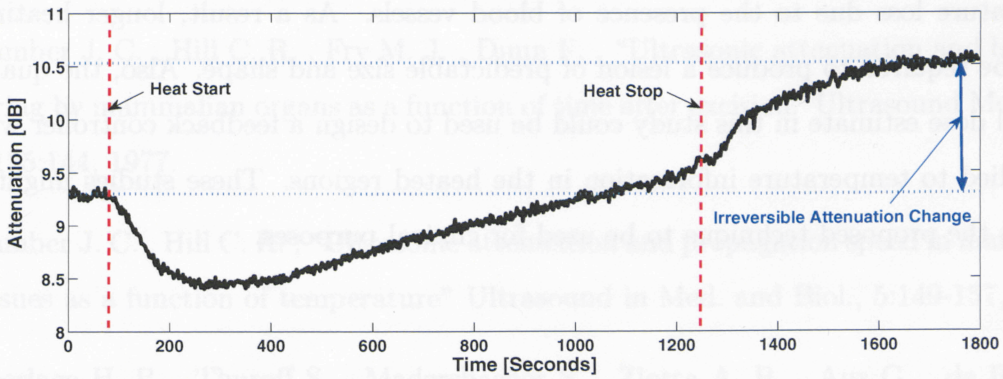

(b) The average attenuation change for bovine liver tissue as a result of performing four separate laser heating experiments.

Figure 4.1: The graphs show the irreversible attenuation increase as a result of protein coagulation in sample of a) albumen and b) bovine liver tissue. The thickness of the each sample was estimated as 2 cm, and that of the lesion 0.7 cm.

In-vivo laser heating experiments are hypothesized to cause lower irreversible temperature dependent effects in the first and last stages of a laser heating procedure, as the temperature of the body is 37 °C.

The data were the result of analyzing the 8-bit mean pixel intensities. These experiments could not be repeated for the 14-bit data, as an automatic data acquisition (as with the 8-bit data) was impossible. Moreover, selecting a desirable region of interest and extracting its 14-bit mean pixel intensity was not possible.

These findings are important in the area of thermal therapy monitoring and show that acoustic attenuation is dependent on temperature, but with significant changes occurring only at temperatures above 50 °C, a temperature to be sufficient for the onset of tissue coagulation.

4.2 Future Work

This study was limited to investigating the effects of heat in tissue-mimicking phantoms and in-vitro experiments. The next step would be to extend the applicability of the proposed methodology to in-vivo experiments. A potential complication could be the continuous temperature loss due to the presence of blood vessels. As a result, longer heating times would be required to produce a lesion of predictable size and shape. Also, the quantitative thermal dose estimate in this study could be used to design a feedback controller which can be applied to temperature information in the heated regions. These studies might help to develop the proposed technique to be used for clinical purposes.

Bibliography

[1] Amin Z. , Bown S. G. , Lees W. R. , "Liver tumor ablation by interstitial lasers photocoagulation, review of experimental and clinical studies" Sem. Interventional Radiol., 10: 88-100, 1993

[2] Bamber J. C. , Hill C. R. , Fry M. J. , Dunn F. , "Ultrasonic attenuation and backscattering by mammalian organs as a function of time after excision" Ultrasound Med. Biol., 7:135:144, 1977.

[3] Bamber J. C. , Hill C. R. , "Ultrasonic attenuation and propagation speed in mammalian tissues as a function of temperature" Ultrasound in Med. and Biol., 5:149-157, 1979.

[4] Beerlage H. P. , Thuroff S. , Madersbacher S. , Zlotta A. R. , Aus G. , de Reijke T. M. , de la Rosette J. J. , "Current status of minimally invasive treatment options for localized prostate carcinoma" Eur. Urol. 37: 213, 2000.

[5] Bowen T. , Connor W. G. , Nasoni R. L. , Pifer A. E. , Sholes R. R. , "Measurement of the temperature dependence of the velocity of ultrasound in soft tissues" Ultrasonic tissue characterization II. Vol. Spec Publ 525. Washington, DC: National Bureau of Standards, US Government Printing Office, pp 57-61, 1979.

[6] Bown S. G. , "Phototherapy of tumors" World Journal of Surgery, 7: 700-709, 1983.

[7] Brettel H. , Roeder U. , Scherg C. , "Ultrasonic transmission camera for medical diagnosis". Biomedizinische Technik 26-63, 1981.

[8] Bush N. L. , Rivens I. , ter Haar G. R. , Bamber J. C. , "Acoustic properties of lesions generated with an ultrasound therapy system" Ultrasound in Med. and Biol., 19: 789-801, 1993.

[9] Carson P. L. , Meyer C. R. , Scherzinger A. L. , "Breast imaging in coronal planes with simultaneous pulse echo and transmission ultrasound" Science, 214:1141-1143, 1981.

[10] Cha C. H. , Lee F. T. Jr. , Gurney J. M. , Markhardt B. K. , Warner T. F. , Kelcz F. , Mahvi D. M. , "CT versus sonography for monitoring radiofrequency ablation in a porcine liver" Am. J. Roentgenol. 175(3):705-711, 2000.

[11] Chen S. S. , Humphrey J. D. , "Heat-induced changes in the mechanics of a collagenous tissue: pseudoelastic behavior at 37C" J. Biomech., 31:211-216, 1998.

[12] Clasen S. , Boss A. , Schmidt D. , Fritz J. , Schraml C. , Claussen C. D. , Pereira P. L. , "Magnetic resonance imaging for hepatic radiofrequency ablation" European Journal of Radiology 59: 140-148, 2006.

[13] Connor C. W. , Hynynen K. , "Bio-acoustic thermal lensing and nonlinear propagation in focused ultrasound surgery using large focal spots: a parametric study" Physicis in Medicine and Biology, 47(11): 1191-1928, 2002.

[14] Damianou C. A. , Sanghvi N. T. , Fry F. J. , "Ultrasonic attenuation of dog tissues as a function of temperature" IEEE Ultrason. Sympos. 1203-1206, 1995.

[15] Damianou C. A. , Sanghvi N. T. , Fry F. J. , Maass Moreno R. , "Dependence of ultrasonic attenuation and absorption in dog soft tissues on temperature and thermal dose" Acoustical society of America, 102(1), pp. 628-634, 1997.

[16] Dickson J. , Calderwood S. , "Thermosensitivity of neoplastic tissue in vivo" Storm F, ed. Hyperthermia in Cancer Therapy. Boston: GK Hall Medical, 63-140, 1983.

[17] Duck F. A. , Baker A. C. , Starritt H. C. , "Ultrasound in Medicine" Institute of Physics Publishing: Bristol and Philadelphia, 1998.

[18] Dupuy D. E. , Goldberg S. N. , "Image-guided radiofrequency tumor ablation: challenges and opportunitiespart 2" J. Vasc. Interv. Radiol. 12:1135-1148, 2001.

[19] Dussik K. T. , "On the possibility of using ultrasound waves as a diagnostic aid" Neurol. Psychiat. 174:153-168, 1942.

[20] Ermert H. , Keitmann O. , Oppelt R. et al , "A new concept for a real-time ultrasound transmission camera" IEEE Ultrasonics Symposium, 2: 1611-1614, 2000.

[21] Fallone B. G. , Moran P. R. , Podgorsak E. B. , "Noninvasive thermometry with a clinical x-ray CT scanner" Med. Phys., 9:715-721, 1982.

[22] Fowlkes J. B. , "Ultrasound Bioeffects and NCRP On Needed US Exposures: The Status of Current Output Limits and Displays" PhD Dissertation, University of Michigan, Michigan, USA, 1999.

[23] Fry W. J. , Wulff V. J. , Tucker D. , Fry F. J. , "Physical factors involved in ultrasonically induced changes in living system" Acoust. Soc. Am., 22:867-876, 1950.

[24] Fry W. J. , Mosberg W. H. , Barnard J. W. , Fry F. J. , "Production of focal destructive lesions in the central nervous system with ultrasound" J. Neurosurg., 11:471-478, 1954.

[25] Gertner M. R. , Wilson B. C. , Sherar M. D. , "Ultrasound properties of liver tissue during heating" Ultrasound Med. Biol., vol.23, no.9, pp. 1395-1403, 1997.

[26] Gertner M. R. , Wilson B. C. , Sherar M. D. , "High-frequency ultrasound properties of multicellular spheroids during heating" Ultrasound Med. Biol.,24:461-468, 1998.

[27] Goldberg S. N. , Gazelle G. S. , Mueller P. R. , "Thermal Ablation Therapy for Focal Malignancy, A Unified Approach to Underlying Principles, Techniques, and Diagnostic Imaging Guidance" Am. J. Roentgenol., 174: 323-331, 2000.

[28] Goldberg S. N. , Dupuy D. E. , "Image-guided radiofrequency tumor ablation: challenges and opportunities-part I" Vasc. Interv. Radiol., 12:1021-1032, 2001.

[29] Goldberg S. N. , Clement J. , Cardella J. F. et al , "Image-guided tumore ablation: standardization of terminology and reporting criteria" J. Vasc. Interv. Radiol., 16:765-778, 2005.

[30] Green P. S. , Ostrem J. S. , Whitehurst T. K. , "Combined reflection and transmission ultrasound imaging" Ultrasound in Med. Biol., 17:283-289, 1991.

[31] ter Haar G. R. , "Ultrasound focal beam surgery" Ultrasound Med. Biol. 21:1089-1100, 1995.

[32] Hynynen K. , "The threshold for thermally significant cavitation in dog's thigh muscle in vivo" Ultrasound Med Biol, 17:157-169, 1991.

[33] Hynynen K et al , "MRI guided non-invasive ultrasound surgery" Med. Phys., 20:107-115, 1993.

[34] Iizuka M. N. , Sherar M. D. , Vitkin I. A. , "Optical phantom materials for near infrared laser photocoagulation studies" Lasers in Surgery and Medicine, 25, 159-169, 1999.

[35] Iizuka M. N. , Vitkin A. , Kolios M. C. , Sherar M. D. , "The effects of dynamic optical properties during interstitial laser photocoagulation" Phys. Med. Biol., 45:1335-1357, 2000.

[36] Ishihara Y. , Calderon A. , Watanabe H. et al , "A precise and fast temperature mapping method using water proton chemical shift" Proceedings of the 11th Annual Meeting of SMRM, Berlin, pp. 4803, 1992.

[37] Jain M. , "A thermal dose controller for laser interstitial thermal therapy" Master's Thesis, Ryerson University, Toronto, Canada, 2006.

[38] Jenne J. W. , Bahner M. , Spoo J. et al , "CT on-line monitoring of HIFU therapy" IEEE Ultrasonics Symposium Proceedings, pp. 1377-1380, 1997.

[39] Jeong J. W. , Kim T. S. , Shin D. C. , Do S. , Singh M. , Marmarelis V. Z. , "Soft Tissue Differentiation Using Multiband Signatures of High Resolution Ultrasonic Transmission Tomography" IEEE Transactions on Medical Imaging, VOL. 24, NO. 3, 2005.

[40] Jolesz F. A. , Silverman S. G. , "Interventional magnetic resonance therapy" Semin. Interv. Radiol., 12:20-27, 1995.

[41] Keitmann O. , Benner L. , Tillig B. , Sander V. , Ermert H. , "New development of an ultrasound transmission camera" Acoustical Imaging, Vol. 26:397-404, 2002.

[42] Kennedy J. , ter Haar G. , Cranston D. , "High intensity focused ultrasound: surgery of the future?" Br. J. Radiol., 76 (909): 590-9, 2003.

[43] King R. L. , Clement G. T. , Maruvada S. , Hynynen K. , "Preliminary results using ultrasound transmission for image-guided thermal therapy" Ultrasound in Medicine and Biology, 29: 293-299, 2003.

[44] Lasser M. E. , Harrison G. H. , Agarwal M. , "Acoustic microscopy for non-destructive semiconductor package evaluation" international symposium on microelectronics, pp. 82-86, 1996.

[45] Lasser M. , "A novel high speed, high resolution, ultrasound imaging system" composites for the real world, pp. 179-185, 1997.

[46] Lele P. P. , "Production of deep focal lesions by focused ultrasound-current status" Ultrasonics , 5:105-122, 1967.

[47] Lo S. B. , Liua C. C. , Freedmana M. T. , Kula J. , Lasser B. , Lasser M. E. , Wang Y. , "Transmission and Reflective Ultrasound Images using PE-CMOS Sensor Array" Ultrasonic Imaging and Signal Processing, Proc. of SPIE Vol. 5750, 2005.

[48] Lu M. D. , Chen J. W. , Xie X. Y. , "Hepatocellular carcinoma: US-guided percutaneous microwave coagulation therapy" Radiology, 221:167-172, 2001.

[49] Miller M. W. , Ziskin M. C. , "Biological consequences of hyperthermia" Ultrasound in Med. and Biol., 15:707-722, 1989.

[50] Mudry K. M. , Plonsey R. , Bronzino J. D. , Biomedical imaging (Principles and applications in engineering), Boca Raton, Fla.: CRC Press, 2003.

[51] Murat F. J. , Poissonier L. , Gelet A. , "Recurrent Prostate Cancer After Radiotherapy - Slavage Treatment by High Intensity Focussed Ultrasound", 2006.

[52] Ophir J. , "Estimation of the speed of ultrasound propagation in biological tissues: a beam-tracking method" IEEE Transactions on Ultrasonics, Ferroelectrics, and Frequency Control, UFFC-33:359-368, 1986.

[53] Oppelt R. , Ermert H. , "Transfer function analysis of a quasioptical ultrasonic imaging system" Ultrasonic Imaging, vol. 6, S. 324-341, 1984.

[54] Parker K. J. , "Ultrasonic attenuation and absorption in liver tissue" Ultrasound in Med. and Biol., 9:363-369, 1989.

[55] Parmar N. , Kolios M. , "An investigation of the use of transmission ultrasound to measure acoustic attenuation changes in thermal therapy" Med., Biol., Eng., Comput., 44, 7, 583-591, 2006.

[56] Peters R. D. , Hinks R. S. , Henkelman R. M. , "Ex vivo tissue-type independence in proton-resonance frequency shift MR thermometry" Magn. Reson. Med., 40(3):454-9, 1998.

[57] Pinkerton J. M. M. , "The absorption of ultrasonic waves in liquids and its relation to molecular constitution" Proc. Phys. Soc., B62: 129-141, 1949.

[58] Prakash O. , Fabbri M. , Drocourt M. , Escanye J. M. , Marchal C. , Gaulard M. L. , Robert J. , "Hyperthermia induction and its measurement using ultrasound" In: Proceedings of IEEE Symposium on Ultrasonics. vol. 80:1689-9. New York: IEEE Press, pp: 1063-1066, 1980.

[59] Rajagopalan B. , Greenleaf J. F. , Thomas P. J. , Johnson S. A. , Bahn R. C. , "Variation of acoustic speed with temperature in various excised human tissues studied by ultrasound computerized tomography" In: Linzer M, editor. Ultrasonic tissue characterization II. Vol. Spec Publ 525. Washington, DC: National Bureau of Standards, US Government Printing Office, pp 227-233, 1979.

[60] Righetti R. , Kallel F. , Stafford R. J. , Price R. E. , Krouskop T. A. , Hazle J. D. , Ophir J. , "Elastographic characterization of HIFU-induced lesions in canine livers" Ultrasound in Med. and Biol., Vol. 25, No. 7, 1099-1113, 1999.

[61] Robinson T. C. , Lele P. P. , "An analysis of lesion development in the brain and in plastics by high-intensity focused ultrasound at low megahertz frequencies" J. Acoust. Soc. Am., 51: 1333-1351, 1972.

[62] Roux F. X. , Merienne L. , Leriche B. , Lucerna S. , Turak B. , Devaux B. , Chodkiewixz J. P. , "Laser interstitial thermotherapy in stereotactical neurosurgery" Lasers Med. Sci. 7:1216, 1992.

[63] Sapareto S. A. , Dewey W. C. , "Thermal dose determination in cancer therapy" Int J Radiat Oncol Biol Phys, 10:787-800, 1984.

[64] Seki T. , Tamai T. , Nakagawa T. , "Combination therapy with transcatheter arterial chemoembolization and percutaneous microwave coagulation therapy for hepatocellular carcinoma" Cancer, 89:1245-1251, 2000.

[65] Shock S. A. , Meredith K. , Warner T. F. , "Microwave ablation with loop antenna: in vivo porcine liver model" Radiology, 231:143-149, 2004.

[66] Siebers S. , Scheipers U. , Welp C. , Werner J. , Ermert H. , "Ultrasound Based Methods For Thermal Therapy Monitoring" Proceedings of the 3rd Symposium on Therapeutic Ultrasound (ISTU3), 2003.

[67] Sokolvo S. Y. , "On the problem of the propagation of ultrasonic oscillations in various bodies" Elek. Nachr. Tech., 6:454-460, 1929.

[68] Straube W. L. , Arthur R. M. , "Theoretical estimation of the temperature dependence of backscattered ultrasonic power for noninvasive thermometry" Ultrasound in Medicine and Biology, 20:915-922, 1994.

[69] Thomsen S. , Pearce J. A. , Cheong W. F. , "Changes in birefringence as markers of thermal-damage in tissues" IEEE Transactions on Biomedical Engineering, 12:1174-1179, 1989.

[70] Watkin N. A. , ter Haar G. R. , Morris S. B. , Woodhouse C. R. J. , "The urological applications of focused ultrasound surgery" Br. J. Urol., 75(Suppl.1):1-8, 1995.

[71] Worthington A. E. , Trachtenberg J. , Sherar M. D. , "Ultrasound properties of human prostate tissue during heating" Ultrasound in Medicine and Biology, 28, 10, 1311-1318, 2002.

[72] Wu F. , Wang Z. B. , Cao Y. De , Chen W. Z. , Bai J. , Zou J. Z. , Zhu H. , "A randomised clinical trial of high-intensity focused ultrasound ablation for the treatment of patients with localised breast cancer" British Journal of Cancer 89: 2227-2233, 2003.

[73] Yang R. , Sanghvi N. T. , Rescorla F. J. , Kopecky K. K. , Grosfeld J. L. , "Liver cancer ablation with extracorporeal high-intensity focused ultrasound" Eur. Urol. 23:17-22, 1993.